nature communications

Article

https://doi.org/10.1038/s41467-025-56866-y

Control of plasma membrane-associated actin polymerization specifies the pattern of the cell wall in xylem vessels

Received: 10 July 2024

Accepted: 25 January 2025

Published online: 26 February 2025

Check for updates

Saku T. Kijima[1,2,3], Takema Sasaki[1], Yuichiro Kikushima[1], Daisuke Inoue[4], Shingo Sakamoto[2,3], Yuki Kondo[5], Soichi Inagaki[6], Masatoshi Yamaguchi[7], Nobutaka Mitsuda[2,3] & Yoshihisa Oda[1]

Cell wall patterning is central to determining the shape and function of plant cells. Protoxylem and metaxylem vessel cells deposit banded and pitted cell walls, respectively, which enable their distinctive water transport capabilities. Here, we show that the pitted cell wall pattern in metaxylem vessels is specified by transcriptional control of actin polymerization. A newly isolated allele of *KNOTTED-LIKE HOMEOBOX TRANSCRIPTION FACTOR 7* (*KNAT7*) was associated with the formation of banded cell walls in metaxylem vessels. Loss of *KNAT7* caused misexpression of *FORMIN HOMOLOGY DOMAIN CONTAINING PROTEIN11* (*FH11*) in the metaxylem, which in turn caused rearrangements of ROP GTPases and microtubules in banded patterns. FH11 function required its plasma membrane anchoring and actin polymerization activity. These results suggest that excessive actin polymerization at the plasma membrane abolishes the pitted cell wall formation and promotes banded cell wall formation in metaxylem vessels. This study unveils the importance of proper control of actin polymerization for cell wall pattern determination.

Cellulose in cell walls is the primary determinants of plant cell shape and function. The rigid cellulose microfibrils in the primary cell wall limit the direction of cell growth by restricting cell expansion. Some types of cells, including xylem cells, deposit a thick lignified secondary cell wall beneath the primary cell wall as a physical reinforcement[1,2]. The secondary cell walls deposited by xylem vessel elements have distinctive patterns, being banded in the protoxylem and pitted in the metaxylem[3,4]. Banded secondary cell walls support the vessel cavity mechanically but are elastic, enabling tissue growth and deformation. Pitted cell walls offer a higher level of stiffness than banded cell walls but restrict the pathways for xylem sap transport to the pits.

Cortical microtubules direct cell wall deposition by tethering cellulose synthase complexes[5,6]. Several microtubule-related proteins modify the patterns of deposition in secondary cell walls in xylem vessels. The MIDD1-Kinesin-13A complex regulates pit size and gap width in secondary cell walls by promoting microtubule depolymerization[7–10]. A Rho/Rac GTPase, ROP11, is activated locally to recruit MIDD1 prior to secondary cell wall deposition[3,10,11]. The GTPase-activating proteins, ROPGAP3 and ROPGAP4, and the guanine nucleotide exchange factors, ROPGEF4 and ROPGEF7, regulate the size and number of spots of activated ROPs on the plasma membrane, which, ultimately, determines the size and number of pits[8,11]. The

[1]Department of Biological Science, Graduate School of Science, Nagoya University, Furo-cho, Chikusa-ku, Nagoya, Aichi 464-8602, Japan. [2]Bioproduction Research Institute, National Institute of Advanced Industrial Science and Technology (AIST), 1-1-1 Higashi, Tsukuba, Ibaraki 305-8566, Japan. [3]Global Zero-Emission Research Center, National Institute of Advanced Industrial Science and Technology (AIST), Tsukuba, Japan. [4] Faculty of Design, Kyusyu University, 4-9-1 Shiobaru, Minami-ku, Fukuoka 815-8540, Japan. [5]Department of Biological Sciences, Graduate School of Science, Osaka University, 1-1 Machikaneyama, Toyonaka, Osaka 560-0043, Japan. [6]Department of Biological Sciences, Graduate School of Science, The University of Tokyo, 7-3-1 Hongo, Bunkyo-ku, Tokyo 113-0033, Japan. [7]Graduate School of Science and Engineering, Saitama University, 255 Shimo-Okubo, Sakura-ku, Saitama 338-8570, Japan.
e-mail: oda.yoshihisa.w5@f.mail.nagoya-u.ac.jp

microtubule-associated proteins IQD13 and CORD1 determine the oval shape of pits by stabilizing and destabilizing the microtubule-plasma membrane interaction, respectively[12,13]. MAP70-5 and MAP70-1 direct the development of cell wall ingrowth at pit boundaries[14,15]. MAP20, another microtubule-associated protein, regulates pit size in *Brachypodium*[16]. A microtubule-severing protein, KTN1, together with microtubule-nucleation proteins, facilitates the regular band pattern found in cell walls in protoxylem vessels[17,18].

Actin filaments also contribute to secondary cell wall development in xylem vessels. In differentiating tracheary elements in cultured Zinnia mesophyll cells, disruption of actin filaments by cytochalasin B changed the band pattern of secondary walls from transverse to longitudinal[19]. In Arabidopsis xylem vessels, actin filaments transport cellulose synthase complexes to the plasma membrane beneath the ingrowing secondary cell walls[20]. The actin-binding protein WAL is recruited to the pits by the active ROP-BDR complex and accumulates actin filaments in pits to promote secondary cell wall deposition at pit boundaries[21].

Although the process of pattern formation in the secondary cell wall through modification of the size and number of pits and gaps is well understood, far less is known about how the different types of secondary cell walls, including their characteristic pitted or banded patterns, are specified in protoxylem and metaxylem vessels. The gradient of expression levels of HD-ZIPIII transcription factors across the radial axis determines the fate of protoxylem and metaxylem cells in the roots of the model plant Arabidopsis (*Arabidopsis thaliana*)[22,23]. The transcription factors VASCULAR-RELATED NAC DOMAIN 6 (VND6) and VND7 induce differentiation of metaxylem- and protoxylem-like vessel elements, respectively[24], although VND7 is also involved in the differentiation of all types of xylem vessels, including both protoxylem and metaxylem[25]. The cellular factors that determine the type of microtubules and cell walls, and thus determine the patterns of pits or bands, have not yet been identified.

In this study, we reveal a novel mechanism by which the control of actin polymerization activity specifies the cell wall pattern. We identified a novel mutant of *KNOTTED-LIKE HOMEOBOX TRANSCRIPTION FACTOR 7* (*KNAT7*) that formed banded cell walls in the root metaxylem. KNAT7 regulates the expression of secondary cell wall biosynthetic genes in fibers[26–31]. Neither the targets of KNAT7 in xylem vessels nor the roles of those genes controlling secondary cell wall patterns have been investigated. The mutant phenotype of *knat7* resulted from the misregulation of *FORMIN HOMOLOGY DOMAIN-CONTAINING PROTEIN 11* (*FH11*). The formin homology (FH) domain has a conserved role in promoting actin polymerization at the barbed ends of actin filaments in eukaryotes[32–34]. Ectopic expression of *FH11* in metaxylem vessels switched the cell wall pattern from pitted to banded. FH11 localized to the plasma membrane and promoted actin polymerization. Following *FH11* expression, the distribution of activated ROP GTPases changed from the metaxylem pattern to that of the protoxylem. Knockout of several *FH* genes resulted in partially disordered secondary cell wall bands in protoxylem vessels, suggesting that actin polymerization by formin was required for the formation of banded cell walls. Transcriptional control of the formin-actin polymerizer was therefore critical for the formation of the pitted cell wall pattern in metaxylem vessels.

Results

KNAT7 suppresses *FH11* to prevent the development of banded cell walls in metaxylem vessels

To identify genes that specified the cell wall pattern in xylem vessels, we screened M2 seeds from an ethyl methanesulfonate (EMS)-mutagenized population of Arabidopsis (*Arabidopsis thaliana*) by differential interference contrast (DIC) microscopy of cleared roots. This isolated #77-41, a mutant that exhibited banded, rather than pitted, cell walls in its metaxylem cell files (Fig. 1a, b). We evaluated the banded/pitted pattern by scoring the longitudinal/transverse ratio of the mean standard deviation of pixel intensity. Scores over 1.0 indicated a banded pattern, whereas scores 0.5–0.8 indicated a pitted pattern (see Methods). Mutant #77-41 had a higher score than wild-type plants (Fig. 1c), indicating the presence of banded cell walls in its metaxylem vessels. Following three backcrosses with wild-type plants, whole-genome sequencing of #77-41 was performed. The mutant harbored a G812A point mutation in the *KNAT7* locus, resulting in an R271H substitution in the homeobox domain of KNAT7 (Fig. 1a). The *knat7* (SALK_002098), a T-DNA insertion line for *KNAT7*, also produced banded cell walls in its metaxylem vessels (Fig. 1b, c). Expression of *KNAT7pro:KNAT7-YFP* in *knat7* and #77-41 restored the wild-type phenotype (Fig. 1b, c; Supplementary Fig. 1), demonstrating that loss of *KNAT7* was responsible for the altered cell wall pattern in metaxylem vessels in *knat7*. Since the *knat7* T-DNA mutant has been frequently used to analyze *KNAT7* function in previous studies[29,35], we used the *knat7* for further analysis of the *KNAT7* function.

To identify the genes responsible for altering the cell wall pattern in *knat7* xylem vessels, we performed an RNA-seq analysis of *knat7*. We used in vitro cultures of hypocotyls[13,36] and cotyledons[37] because the population of differentiating xylem cells in intact roots is tiny and these methods efficiently induce ectopic differentiation of xylem vessel elements. We identified differentially expressed genes (DEGs) that were up-or down-regulated in *knat7* relative to their expression in the complementation line (*knat7* harboring *KNAT7pro:KNAT7-EYFP*; Supplementary Fig. 2a, b; Supplementary Data 2 and 3).

Expression of the HD-ZIPIII transcription factors, *ATHB8*, *PHABULOSA, CORONA*, and *REVOLUTA*, which determine protoxylem/metaxylem cell fate, was not affected in *knat7* ($P = 0.22–0.76$), indicating that the cell fate of xylem cells was unaltered. The DEGs of *knat7* included the cell wall-related genes, *IRX10*, *IRX14-L*, *LAC5*, *MYB54*, and cytoskeleton-related genes, *MAP70-5* and *TPXL6* (Supplementary Table 1). Expression levels of some *knat7* DEGs were also affected in the #77-41 mutant (Supplementary Fig. 2c), suggesting that the R271H substitution in #77-41 impaired the transcriptional activity of KNAT7. Of these, we focused on *FORMIN HOMOLOGY DOMAIN-CONTAINING PROTEIN 11* (*FH11*), which was upregulated 1.51- and 2.61-fold in cultured *knat7* cotyledons and hypocotyls, respectively.

To test whether *FH11* was involved in producing the *knat7* phenotype, an *FH11* T-DNA insertion line GABI_348C07, hereafter *fh11* (Fig. 1a), was crossed with *knat7*. Metaxylem vessels in the *knat7 fh11* double mutant developed pitted cell walls, resembling those seen in wild-type plants (Fig. 1b, c). *fh11* therefore suppressed the *knat7* phenotype. Introducing *FH11pro:FH11-EYFP* into the *knat7 fh11* double mutant reproduced the banded cell wall phenotype like *knat7* mutant (Fig. 1b, c), indicating that the *FH11* disruption in *fh11* mutant was responsible for the suppression of the *knat7* phenotype by *fh11*. These results suggest that *knat7* affected cell wall patterning through the *FH11* function in metaxylem vessels.

To determine the pattern of *FH11* expression, *FH11pro:FH11-EYFP* was observed in wild-type and *knat7* roots. In wild-type roots, FH11-EYFP was detected in protoxylem vessels, but not in metaxylem vessels. By contrast, FH11-EYFP was observed in both protoxylem and metaxylem vessels in *knat7* roots (Fig. 1d, e). This suggests that *KNAT7* suppressed *FH11* expression specifically in metaxylem vessels, and thus that loss of *KNAT7* caused misexpression of *FH11* in the metaxylem. To investigate the effects of misexpressing *FH11* in metaxylem vessels, *FH11-tagRFP* was placed under the control of a xylem-specific promoter, *IRREGULAR XYLEM3* (*IRX3*)[38], and expressed in wild-type plants. The transformants carrying *IRX3pro:FH11-tagRFP* developed metaxylem vessels with banded cell walls, similar to those of *knat7* (Fig. 1b, c), indicating that *FH11* expression in metaxylem vessels was sufficient to induce banded cell wall formation. Taken together, these results led us to conclude that *KNAT7* suppressed expression of *FH11* in metaxylem vessels, and thus that loss of *KNAT7* resulted in *FH11*

https://doi.org/10.1038/s41467-025-56866-y

misexpression, which in turn promoted the development of banded cell walls.

To test whether the KNAT7 suppresses *FH11* promoter activity, an effector-reporter assay[39] was conducted using Arabidopsis leaf protoplasts (Supplementary Fig. 3). The 1 kbp- and 2 kbp-length upstream sequences from the *FH11* start codon were fused to the luciferase reporter (*FH11pro1k:Luc* and *FH11pro2k:Luc*). These reporters were less active in the presence of KNAT7 effector (*35S:KNAT7*) than in the presence of the negative control effector (*35S:VAMP722*) (Supplementary Fig. 3), suggesting that KNAT7 suppressed the transcriptional activity of *FH11* promoter.

In stems, *KNAT7* acts with *KNAT3* during the development of secondary cell walls[30,31]. The metaxylem vessels of *knat3*, a *KNAT3* T-DNA insertion line (SALK_136464), developed pitted cell walls,

Fig. 1 | KNAT7 and FH11 regulate cell wall patterns in root metaxylem vessels. **a** Diagram showing locations of T-DNA insertions and a mutation in the *knat7*, *knat3*, and *fh11* mutants. **b** Differential interference contrast (DIC) microscopy images of metaxylem vessels in roots of wild-type (WT), #77-41, *knat7*, *knat7* harboring *KNAT7pro:KNAT7-EYFP* (*knat7* + *KNAT7*), *fh11*, *IRX3pro:FH11-tagRFP* (*FH11 ox*), *knat7 fh11*, *knat7 fh11* harboring *FH11pro:FH11-EYFP* (*knat7 fh11* + *FH11*), *knat3*, and *knat3 knat7* plants. Red arrowheads indicate metaxylem vessels; blue arrowheads indicate protoxylem vessels. Scale bars = 5 μm. **c** Aspect ratio of deviation of brightness along the horizontal and vertical axes of metaxylem vessels. Asterisks indicate significant differences between WT and each line by one-way ANOVA with Dunnett's post hoc test; $n = 15$ plants; *: $P < 0.0001$; ns: no significant difference. **d** FH11-EYFP (*FH11pro:FH11-EYFP*) expression in the cortex of protoxylem (proto) and metaxylem (meta) vessels in roots of WT, *knat7*, and *knat3 knat7* plants. Scale bars = 5 μm. **e** Intensity of FH11-EYFP (*FH11pro:FH11-EYFP*) fluorescence. Box plots indicate the median (horizontal line), interquartile range (25% to 75%), and the minimum and maximum of the data (whiskers); dots are individual data points. Asterisks indicate significant differences by one-way ANOVA with Tukey's test; $n = 14$ (WT), 15 (*knat7*), 16 (*knat3 knat7*) cells in protoxylem, $n = 15$ cells in metaxylem; *: $P < 0.05$, ****: $P < 0.0001$; ns: no significant difference.

similar to those of wild-type plants. By contrast, the metaxylem vessels in the *knat3 knat7* double mutant formed banded cell walls comparable to those of *knat7*, which suggests that *KNAT3* was not involved in cell wall patterning in the metaxylem (Fig. 1b, c). It has previously been reported that xylem vessels are collapsed in *knat7* stems[28,40]. In the current study, the stems of *knat7 fh11* double and *knat7* single mutants exhibited similarly collapsed xylem phenotype, suggesting that *FH11* was not involved in *KNAT7* function in stems (Supplementary Fig. 4). The *knat7*, *knat3 knat7* and *FH11*-expressing (*IRX3pro:FH11-EYFP*) plants developed leaves, stems and roots to the size comparable to those of wild-type plants (Supplementary Fig. 5), suggesting that the altered patterning of secondary cell walls had little effect on plant development under the normal growth condition.

The secondary cell wall pattern was not affected in the protoxylem vessels of the *knat7* plants and FH11-expressing plants (*IRX3pro:FH11-tagRFP*), although the cell width and the cell wall bands of the protoxylem vessels were thinner and sparser, respectively, in the mutants than in wild-type plants (Fig. 1b). We therefore focused on the effects of *knat7* and *FH11* on the secondary cell wall pattern in metaxylem vessels.

Misexpression of FH11 reorganizes the cytoskeleton of the metaxylem into a protoxylem-like pattern

Cell wall patterning in xylem vessels is directed by the cytoskeleton. The structure of the cytoskeleton was altered in *knat7* mutants and *FH11*-expressing plants in a manner consistent with the changes in their cell walls. Microtubules (*IRX3pro:EYFP-TUB6*) in wild-type metaxylem cells were aligned beneath the secondary cell walls and accumulated in pit boundaries (Fig. 2a; Supplementary Fig. 6). By contrast, bands of transverse microtubule formed in the metaxylem cells of *knat7* and *FH11*-expressing (*IRX3pro:FH11-tagRFP*) plants that showed a distribution resembling that seen in protoxylem cells of wild-type plants (Fig. 2a; Supplementary Fig. 6). The close observation of FH11-expressed metaxylem showed that FH11 was localized to the plasma membrane but was absent from the area occupied by cortical microtubules, resulting in the mutually exclusive localization of FH11 and microtubules (Supplementary Fig. 7).

Actin filaments were also affected in *knat7* mutants and *FH11*-expressing plants. In the metaxylem cells of wild-type plants, actin filaments (*MIDD1pro:Lifeact-mGFP*) formed circular bands in pits and actin cables running along the longitudinal axis (Fig. 2b; Supplementary Fig. 8). This was consistent with the previous report that the ROP-BDR-WAL complex promotes actin filament assembly at pit boundary[21]. Although longitudinal actin cables were observed in metaxylem vessels in *knat7* mutants and *FH11*-expressing (*IRX3pro:FH11-tagRFP*) plants, the circular actin bands did not form. Instead, weak fluorescence of Lifeact-mGFP was observed at the cell cortex. These patterns of actin distribution resembled those in the protoxylem cells in wild-type plants (Fig. 2b; Supplementary Fig. 8). The weak fluorescence of Lifeact-mGFP at the cell cortex was more evident in *FH11*-expressing plants than in *knat7*; in addition, the actin cables were less evident in *FH11*-expressing cells than in *knat7* (Supplementary Figs. 8, 9). These differences between *knat7* and FH11-expressing cells probably resulted from the higher levels of *FH11* present in *FH11*-expressing cells (Supplementary Fig. 9e). At the middle stage of the FH11-expressed metaxylem cells, the fluorescence of the mGFP-Lifeact and FH11-tagRFP was uniformly localized at the cell cortex (Supplementary Fig. 9c, d). At the late stage, however, these fluorescence became more evident at the narrow transverse bands, which were the gaps of microtubules (Supplementary Fig. 9c, d).

To analyze the localization of microtubules and actin filaments in detail, we observed cultured hypocotyl cells in which large epidermal cells had differentiated ectopically into metaxylem vessels[13,36]. Consistent with the phenotype observed in roots, hypocotyl cells from *knat7* mutants and *FH11*-expressing (*IRX3pro:FH11-tagRFP*) plants formed banded cell walls, whereas wild-type cells developed pitted cell walls. Likewise, banded microtubules formed instead of the pitted microtubule array in *knat7* and *FH11*-expressing cells (Supplementary Fig. 10a). Fine actin networks at the cell cortex and fewer actin cables were observed in *knat7* and *FH11*-expressing cells (Supplementary Fig. 10b). These results suggest that *FH11* expression reorganizes the cytoskeleton of metaxylem cells into a protoxylem-like form. Consistent with the observations in the root metaxylem cells, FH11 and microtubules were localized at the plasma membrane, but they were mutually exclusive (Supplementary Fig. 10c), and the cortical actin filaments were preferentially localized to the area where FH11 existed (Supplementary Fig. 10d).

FH11 promotes polymerization of actin filaments beneath the plasma membrane

To investigate how FH11 reorganized the cytoskeleton, we characterized the subcellular localization of FH11 and the effect of ectopic *FH11* expression. The FH11 protein consists of a N-terminal signal peptide, a transmembrane domain, and a conserved dimeric FH1-FH2 domain which promotes actin polymerization via enzymatic activity (Fig. 3a)[41]. FH11-EYFP (*LexApro:FH11-EYFP*), expressed under the control of an estrogen-induced promoter, *Locus for X-ray sensitivity A* (*LexA*)[42], localized to the plasma membrane (labeled with FM4-64) in cultured Arabidopsis cells (Fig. 3b). The association of FH11 with the plasma membrane was confirmed in plasmolyzed cells (Fig. 3c). A truncated form of FH11 that lacked the signal peptide and the transmembrane domain (251–884 aa) localized to the cytoplasm, whereas a truncated FH11 without the FH1-FH2 domain (1–400 aa) remained at the plasma membrane, indicating that the transmembrane domain anchored FH11 to the plasma membrane (Fig. 3b). Localization of FH11 at the plasma membrane was also observed in roots of *FH11*-expressing plants (Supplementary Figs. 7, 9c).

Since FH11 contains the conserved FH1-FH2 domain, we expected FH11 to promote actin polymerization at the plasma membrane. *FH11-tagRFP* was expressed under the control of an estrogen-induced promoter in root epidermal cells expressing *UBQ10pro:Lifeact-mGFP*. Lifeact-mGFP was observed using spinning disk confocal microscopy 24 h after the onset of estrogen treatment. The density of the fine actin filaments at the cell cortex increased in the *FH11*-expressing (*LexApro:FH11-tagRFP*) cells, and the number of longitudinal actin cables reduced, as indicated by a reduction in skewness of the intensity histogram (Fig. 3d–f). To detect actin filaments in the vicinity of the plasma membrane, we observed hypocotyl epidermal cells using variable angle

https://doi.org/10.1038/s41467-025-56866-y

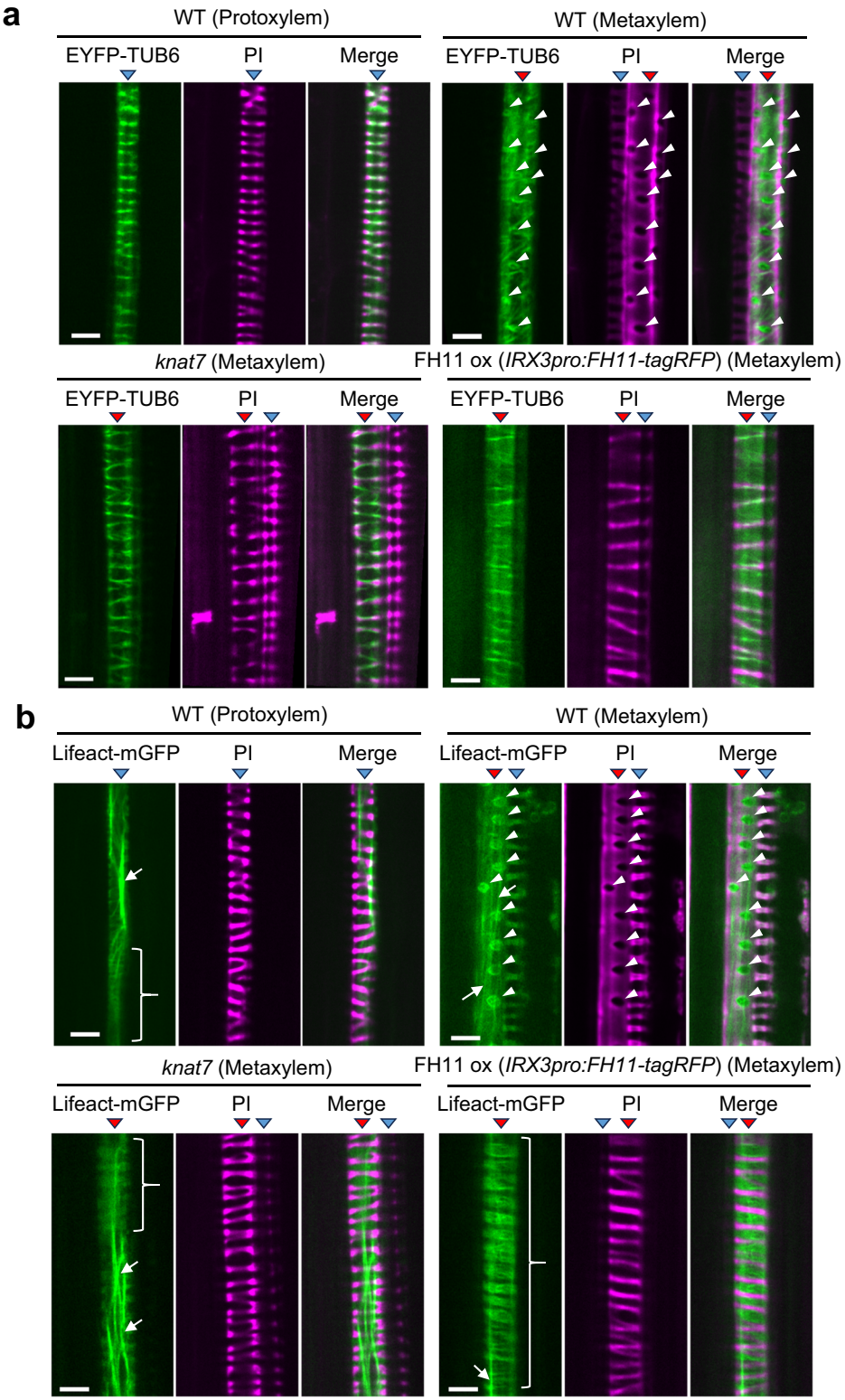

Fig. 2 | The alignment of the cytoskeleton in metaxylem cells in *knat7* and FH11-expressing plants resembles that in protoxylem vessels. a and **b** Microtubules (*IRX3pro:EYFP-TUB6*) (**a**) and actin filaments (*MIDD1pro:Lifeact-mGFP*) (**b**) in protoxylem and metaxylem vessel cells of wild-type (WT), *knat7*, and FH11-expressing (FH11 ox, *IRX3pro:FH11-tagRFP*) plants. Cell walls were labeled with propidium iodide (PI). The images are representative of three independent experiments. White arrowheads indicate pits; white arrows indicate actin cables; curly brackets indicate areas of weak fluorescence; red arrowheads indicate metaxylem vessels; blue arrowheads indicate protoxylem vessels. Individual images show the cortex; the corresponding mid-plane sections are shown in Supplementary Figs. 6 and 8. Scale bars = 5 μm.

total internal reflection fluorescence (VA-TIRF) microscopy. Consistent with the confocal microscopy results, the number of fine actin filaments increased in cells expressing *LexApro:FH11-tagRFP* (Supplementary Fig. 11). These results suggest that FH11 promoted actin polymerization at the cell cortex. Given the localization of FH11, the weak Lifeact-mGFP fluorescence observed in *IRX3pro:FH11-tagRFP*-expressing metaxylem cells (Fig. 2b; Supplementary Fig. 9b, c) was probably from fine actin filaments polymerized by FH11 at the plasma membrane. The reduction

https://doi.org/10.1038/s41467-025-56866-y

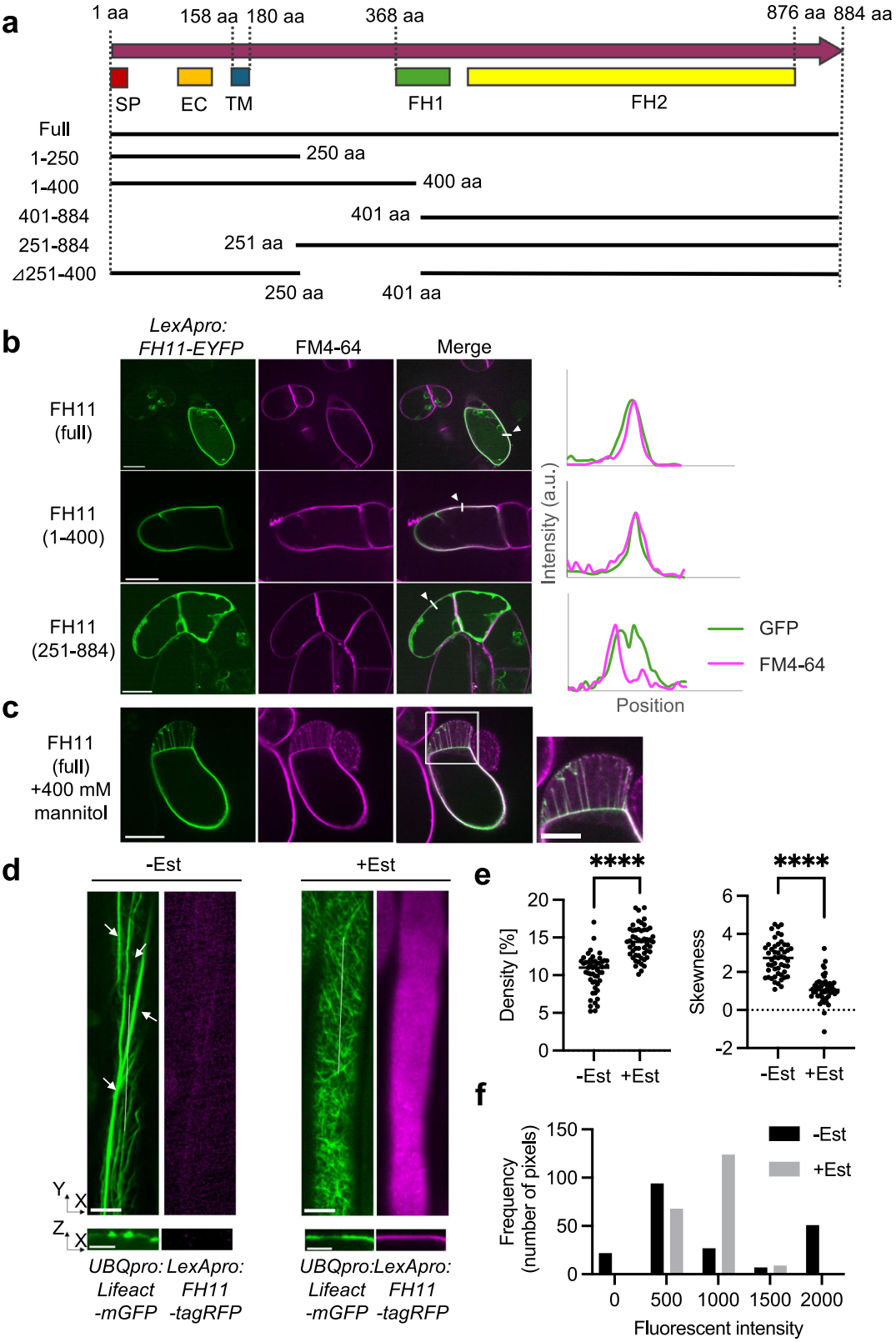

in actin cable formation following *IRX3pro or LexApro:FH11-tagRFP* expression (Figs. 2b, 3d; Supplementary Fig. 9c, 11) probably resulted from the depletion of cytoplasmic actin monomers caused by excessive polymerization of actin filaments at the cell cortex.

The dynamics of actin filaments (*UBQ10pro:Lifeact-mGFP*) in the *LexApro:FH11-tagRFP*-expressed cells, observed by the VA-TIRF microscopy after estrogen treatment, were comparable to those in the control cells without estrogen treatment (Supplementary Fig. 12), suggesting that FH11 did not influence the dynamics of actin filaments.

To investigate the involvement of the different FH11 domains in actin polymerization at the cell cortex, full-length (*UBQ10pro:FH11-tagRFP*) or truncated (*UBQ10pro:FH11(1–400 or 251-884)-tagRFP*) FH11 was expressed together with the *UBQ10pro:Lifeact-mVenus* in the epidermis of *Nicotiana benthamiana* (*N. benthamiana*) leaves. Fine

Fig. 3 | FH11 localizes at the plasma membrane and promotes polymerization of actin filaments. a Diagram of FH11 protein showing truncated fragments. SP, EC and TM indicate the signal peptide, extra-cytoplasmic Ser/Pro rich, and transmembrane domains, respectively. Numbers indicate the locations of amino acid residues relative to the full-length protein. **b** and **c** FH11 (*LexApro:FH11-EYFP*) and plasma membrane (FM4-64) in Arabidopsis cells cultured without (**b**) or with (**c**) 400 mM mannitol. In (**b**), the intensity profiles along the white lines (indicated by white arrowheads) are shown in graphs to the right of each panel. The white box in (**c**) shows Hechtian strands induced by 400 mM mannitol; an enlarged image of this area is shown in the far-right panel. The images are representative of three independent experiments. All scale bars = 20 μm, except for the enlarged image, in which scale bar = 10 μm. **d** Actin filaments (*UBQ10pro:Lifeact-mGFP*) in root epidermal cells harboring *LexApro:FH11-tagRFP* treated with (+Est) or without (-Est) 2 μM estradiol. Arrows indicate actin cables. The lower panels show xz slices along the white lines. Scale bars = 5 μm [xy] or 2.5 μm [xz]. **e** Skewness and density of actin filaments. Dots are individual data points; the horizontal line indicates the median; $n = 51$ (-Est) and 52 (+Est) cells; ****: $P < 0.0001$ (two-tailed Student's t-test). **f** Histogram of fluorescent intensity along the white lines shown in (**d**). Mean values ± standard deviations are Control: 1636.8 ± 2243.3; FH11 (full): 840.8 ± 220.8, (two-tailed Student's t-test, $P = 1.20E\text{-}6$).

actin filaments formed beneath the plasma membrane in cells expressing full-length FH11, but not in cells expressing truncated FH11 that lacked the transmembrane domain (251–884 aa) or the FH1-FH2 domain (1–400 aa) (Supplementary Fig. 13). This indicated that the transmembrane and FH1-FH2 domains of FH11 were responsible for the localization and actin-polymerizing activities of FH11, respectively.

FH11 slightly influences microtubule dynamics

We also analyzed the effects of FH11 expression on cortical microtubules. *UBQ10pro:EYFP-TUB6* and *LexApro:FH11-tagRFP* were observed in root epidermal cells, with or without estradiol treatment. Microtubule alignment was not significantly affected by FH11 expression (Supplementary Fig. 14a-c). Nevertheless, the intensity of EYFP-TUB6 fluorescence decreased following FH11 expression (Supplementary Fig. 14a, d), which probably indicated a reduction in the number of microtubules in each bundle of cortical microtubules.

To further investigate the effects of FH11 on the microtubules, full-length (*UBQ10pro:FH11-tagRFP*) or truncated (*UBQ10pro:FH11(1-400 or 251-884)-tagRFP*) FH11 was expressed together with the *UBQ10-pro:EYFP-TUB6* in the epidermis of *N. benthamiana* leaves. Expressions of full-length and truncated FH11 slightly reduced the density of microtubules (Supplementary Fig. 15a, b) and had little effect on the skewness of the intensity histogram of microtubules (Supplementary Fig. 15c), suggesting that the transmembrane of FH11 affected the amount of cortical microtubules.

To analyze the effects of FH11 on microtubule dynamics, full-length (*UBQ10pro:FH11-tagRFP*) or truncated FH11 (*UBQ10pro:FH11(1-400)-tagRFP*) was expressed together with the microtubule +tip marker, *35Spro:GFP-EB1*, in the epidermis of *N. benthamiana* leaves. The full-length and the N-terminal domain of FH11 reduced the EB1 density and velocity, but the full-length FH11 had greater effects on the EB1 density than the truncated FH11 (Supplementary Fig. 16). These results suggest that FH11 affects microtubule dynamics, although the N-terminal transmembrane domain of FH11 could also slightly influence the microtubule dynamics. Because EB1 associates with the microtubule plus ends during the microtubule growth phase, FH11 might shorten the microtubule growth phase or eliminate cortical microtubules by inhibiting their association with the plasma membrane. In contrast to metaxylem cells, FH11 only slightly affected microtubule alignment in the epidermis (Fig. 2a; Supplementary Figs. 6, 7, 10 and 14-16), implying that the effect of FH11 on microtubule alignment is indirect.

FH11 promotes actin polymerization in the profilin-actin pool

Profilin, an abundant cytoplasmic protein, binds to actin monomers to inhibit actin polymerization[43–46]. The FH1 domain of mammalian formin (mDia1) recruits profilin-actin to the growing barbed end of actin filaments and enables profilin release at the FH2 domain, thereby promoting actin polymerization[47,48]. The FH1-FH2 domain of Arabidopsis FH14 processively promotes actin polymerization in the presence of profilin[49]. To investigate whether a recombinant FH1-FH2 domain of FH11 also promotes polymerization of profilin-actins, actin polymerization was analyzed in vitro using TIRF microscopy. We initially confirmed that Arabidopsis PROFILIN1 (PRF1) inhibited actin polymerization in a concentration-dependent manner (Supplementary Fig. 17a, c). The effect of the FH1-FH2 domain was tested in the presence of 5 μM PRF1. The FH1-FH2 domain of FH11 promoted the polymerization of actin filaments (Supplementary Fig. 17b, d). This finding was consistent with observations in FH11-expressing cells (Fig. 3d, e; Supplementary Figs. 11, 13).

Taken together, the results of these in vivo and in vitro analyses suggest that FH11 promoted actin polymerization beneath the plasma membrane and that FH11 may indirectly influence microtubule alignments through actin polymerization.

Plasma membrane-associated actin polymerization is required for banded cell wall formation in the metaxylem

Truncated FH11 under the control of the *IRX3* promoter was specifically expressed in xylem cells to determine whether cellular activity of FH11 contributed to its ability to alter the pattern in the cell wall. The metaxylem vessels of transgenic plants expressing truncated FH11 lacking either the transmembrane domain (251–884 aa and 401–884 aa) or the FH1-FH2 domain (1–250 aa and 1–400 aa) developed pitted cell walls, whereas vessels in transgenic plants expressing FH11 that lacked the middle region between the transmembrane domain and the FH1-FH2 domain (Δ251–400 aa) developed banded cell walls, as did those expressing full-length FH11 (Fig. 3a; Fig. 4a, b; Supplementary Fig. 18a). This indicated that alteration of the cell wall pattern required both the transmembrane and FH1-FH2 domains of FH11.

To clarify whether the actin polymerization activity of the FH1-FH2 domain was necessary, the mutations I543A or K690D were introduced into FH11; these mutations abolish the interaction of the FH1-FH2 domain with actin filaments[50]. Plants expressing FH11 containing either I543A or K690D or both mutations developed pitted metaxylem vessels (Fig. 4c–e; Supplementary Figs. 18b, c and 19). By contrast, replacing the FH1-FH2 domain with that of human formin DIAPH1 (mDia1)[51,52], a well-characterized actin polymerizer, induced banded cell walls (Fig. 4c–e). These results indicated that the actin-polymerizing activity of FH11 was required to induce the formation of banded cell walls in the metaxylem.

Next, we characterized the N-terminal transmembrane domain of FH11. We introduced modified forms of FH11 in which the transmembrane domain was replaced with a corresponding domain from either human lysosomal protein LAMP1[53] or Arabidopsis RLK (receptor-like kinase 1-like family)[54]. Each modified protein resulted in the formation of banded cell walls in the metaxylem vessels, as did intact FH11 (Fig. 4c–e). Replacement of the N-terminal region of FH11 (1–180 amino acids), which includes the signal peptide, extracellular domain, and transmembrane domain, with RCI2A/LTI6 (low temperature and salt responsive protein family), a 54-amino acid transmembrane polypeptide[55], also resulted in the formation of banded cell walls in metaxylem vessels (Fig. 4c–e). By contrast, replacing the N-terminal region of FH11 with the palmitoylation signal peptide[56] or the N-terminal palmitoylation domain from ARA6[57], which are anchored to the plasma membrane by their lipid modification, resulted in the formation of pitted cell walls with enlarged pits (Supplementary Figs. 18c, 19). These results suggest that a transmembrane structure of FH11 in addition to its localization to the plasma membrane is required for the activity of FH11 to form banded cell walls.

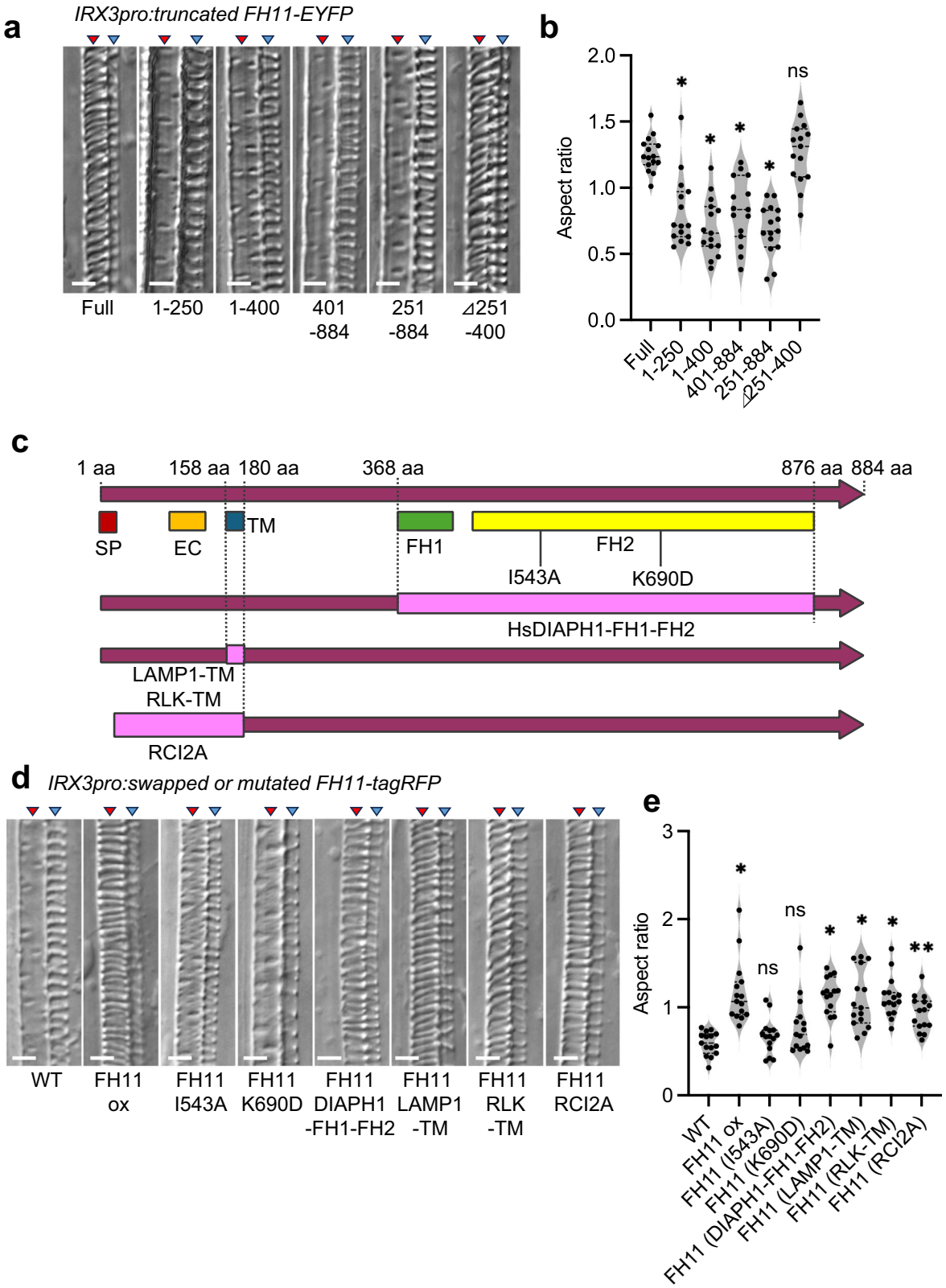

FH11 abolishes the local ROP activation of metaxylem vessels

The pitted cell wall pattern of metaxylem vessels is controlled by ROP signaling[8,11]. ROPs are locally activated in the future pit regions of differentiating metaxylem vessels and promote microtubule depletion. We hypothesized that polymerization of plasma membrane-associated actin filaments by FH11 might modify the pattern of ROP signaling in metaxylem cells to change the pattern of the cell wall. To determine whether ROPs were affected by FH11 expression, *MIDD1pro:MIDD1ΔN-GFP*, a marker for active ROPs[8], was introduced into wild-type, *knat3 knat7*, and *FH11*-expressing (*IRX3pro:FH11-tagRFP*) plants. Spots of active ROPs were observed in all three genotypes during the early stage of metaxylem differentiation. At the late stage, however, the spots were maintained in wild-type cells but active ROPs were distributed widely across the cell cortex in *knat3 knat7* and *FH11-*

Fig. 4 | The transmembrane and FH1-FH2 domains of FH11 are required for the formation of banded cell walls in metaxylem vessels. a DIC images of metaxylem vessels in roots expressing truncated FH11 proteins. The truncated proteins shown in Fig. 3a were fused with EYFP at the C-terminus and expressed under the control of the *IRX3* promoter. Red and blue arrowheads indicate metaxylem and protoxylem vessels, respectively. Scale bars = 5 μm. **b** Aspect ratio of deviation of brightness along the horizontal and vertical axes of metaxylem vessels. Asterisks indicate significant differences between lines expressing full-length (Full, *IRX3-pro:FH11-EYFP*) and truncated FH11 by one-way ANOVA with Dunnett's post hoc test; $n = 15$; *: $P < 0.0001$; ns: no significant difference. **c** Diagram of FH11 proteins containing mutations or domain swaps. Numbers indicate the positions of amino acid residues relative to the beginning of the full-length protein. **d** DIC images of metaxylem vessels in the roots of plants expressing the indicated forms of FH11. Each form of FH11 was fused with tagRFP at the C-terminus and expressed under the control of the *IRX3* promoter. Red and blue arrowheads indicate metaxylem and protoxylem vessels, respectively. Expression of each exogenous FH11 was verified by confocal microscopy (Supplementary Fig. 18). Scale bars = 5 μm. **e** Aspect ratio of deviation of brightness along the horizontal and vertical axes of metaxylem vessels. Asterisks indicate significant differences between wild-type (WT) plants and lines expressing FH11 by one-way ANOVA with Dunnett's post hoc test; $n = 15$; *: $P < 0.0001$; **: $P < 0.005$; ns: no significant difference.

expressing plants (Fig. 5a, b). This indicated that FH11 dispersed the spots of ROP activity in metaxylem cells, causing redistribution of ROPs across the cell cortex. The drastic change in the ROP localization at the late stage was probably due to the increase in the amount of FH11 expressed during the metaxylem differentiation: the amount of FH11 was insufficient to disperse the active ROPs at the early stage of differentiation.

In metaxylem, ROPs are locally activated by the action of ROPGEFs and ROPGAPs, and the activated ROPs are confined within the lattice of cortical microtubules, which inhibits the lateral diffusion of active ROPs[8,11,12]. To test whether the FH11 affects the behavior of active ROPs, we reconstructed the local ROP activation in the presence of the full-length or truncated (1-250) FH11 ectopically in the leaf epidermis of *N. benthamiana*, by introducing the expression of the *ROP11*, *ROPGAP3*, PRONE domain of *ROPGEF4*, and *tagRFP-MIDD1* which can mark both active ROPs and microtubules[8,58]. The MIDD1 localized only to microtubules when MIDD1 was expressed alone, whereas MIDD1 localized to the microtubules and the plasma membrane when expressed with ROP11 whose active form can recruit MIDD1 to the plasma membrane (Supplementary Fig. 20, top panels). When MIDD1 was co-expressed with ROP11, ROPGAP3, and ROPGEF4PRONE, MIDD1 localized to microtubules and the segmented region of the plasma membrane (Supplementary Fig. 20, top panels), because ROPGAP3 and ROPGEF4PRONE activate ROP11 locally at the plasma membrane (Supplementary Fig. 20, top panels). The locally activated ROPs are also confined within the lattice of the cortical microtubules as microtubules inhibit lateral diffusion of activated ROPs along the plasma membrane[8,58].

Then we introduced these four genes together with the truncated FH11 (*LexApro:FH11(1-250)-EYFP*) (Supplementary Figs. 20, middle panels, 21a). The segmented pattern of MIDD1 was observed in 45% of the cells (Fig. 5c; Supplementary Figs. 20, 21). The remaining 55% of the cells formed uniform or partially segmented patterns of MIDD1. By contrast, when the full-length FH11 (*LexApro:FH11-EYFP*) was expressed, only 1% of the observed cells formed the segmented pattern of MIDD1 and the remaining 99% of the observed cells formed uniform or partially segmented pattern of MIDD1 (Fig. 5c; Supplementary Figs. 20, bottom panels, 21b, c). Consistent with this, the mean-variance of tagRFP-MIDD1 intensity within each cell (standard deviation of tagRFP intensity normalized by their mean intensity) of the truncated FH11-expressing cells was higher than those of full-length FH11-expressing cells (Fig. 5d). The expression of FH11 did not affect the localization of MIDD1 when only ROP was co-expressed (Supplementary Fig. 20, middle column). These results suggest that FH11 inhibits local activation of ROP11 induced by ROPGEF4PRONE and ROPGAP3 and/or confinement of active ROP11 by microtubules on the plasma membrane.

To clarify whether the banded cell wall pattern induced by FH11 depended on the spots of active ROPs observed during the early stage, we used CRISPR/Cas9 to introduce the *knat7* mutation into the ROP mutants, *ropgef4 ropgef7* and *ropgap3 ropgap4*; both number of spots of active ROPs and number of pits are reduced in these mutants[11]. We reasoned that, if the spots of active ROPs functioned in pattern formation, the banded cell wall pattern induced by FH11 would be affected in these mutants. The resulting mutants exhibited banded cell wall patterns that were indistinguishable from those of *knat7* (Supplementary Fig. 22), however, indicating that FH11 induced the formation of banded cell walls independently of the spots of active ROPs.

ROP regulates the density of banded cell wall bands in protoxylem vessels through the MIDD1-Kinesin-13A complex[10]. To test whether ROPs in metaxylem expressing FH11 had the same function as those in the protoxylem, a *KNAT7*-knockout mutation was introduced into the *midd1 midd2* double mutant, which forms densely banded cell walls in its protoxylem vessels. The metaxylem vessels of the *knat7 midd1 midd2* triple mutant formed more densely banded cell walls than *knat7*, suggesting that the ROP-MIDD1-Kinesin-13A pathway functions in both the metaxylem and protoxylem vessels of *knat7* (Supplementary Fig. 22). Taken together, our data suggests that misexpression of *FH11* in the metaxylem alters ROP localization, allowing ROPs to function there as in protoxylem vessels.

Formins are required for the organization of cell wall bands in the protoxylem

Since *FH11* was expressed in the protoxylem vessels of wild-type plants (Fig. 1d, e), we hypothesized that *FH11* was involved in determining the type of cell wall patterns in protoxylem vessels. The cell wall bands in the protoxylem vessels of the *fh11* mutant were slightly deformed and tilted, compared with those of wild-type plants (Fig. 6). The Arabidopsis genome encodes 21 *FH* genes, whose functions may be redundant with *FH11*. In addition to *FH11*, four class I formins, *FH5*, *FH6*, *FH7*, and *FH8*, and three class II formins, *FH17*, *FH18*, and *FH20*, are expressed in xylem vessels[59]. We used CRISPR/Cas9 to induce multiple *FH* gene knockouts in *fh11* mutants (Supplementary Fig. 23) and selected lines harboring indel mutations causing frame shifts and premature stop codons. We identified two lines (#28-2, #170-2) of the quadruple mutant *fh11 fh17 fh18 fh20* that had partially deformed banded cell walls in which the bands were connected with the longitudinal cell wall (Fig. 6; Supplementary Fig. 24; Supplementary Table 2); two lines (#9-10, #9-11) of the quintuple mutant, *fh5 fh6 fh7 fh8 fh11*, showed a similar phenotype. Line #136-1 of the sextuple mutant, *fh5 fh7 fh11 fh17 fh18 fh20*, and two lines (#129-21, #131-1) of the septuple mutant, *fh5 fh7 fh8 fh11 fh17 fh18 fh20*, showed an enhanced phenotype (Fig. 6; Supplementary Fig. 24; Supplementary Table 2). The three-dimensional reconstruction and omni-directional projections of protoxylem vessels showed that the mutants formed sparse cell wall bands with uneven spaces in protoxylem vessels (Supplementary Fig. 25). These results suggest that *FH* genes are involved in the organization of the banded cell walls in protoxylem vessels.

Unlike FH11, the overexpression of FH5, FH6, FH7, FH17, FH18, and FH20 in root xylem vessel cells (*pIRX3:FH-EYFP*) did not induce the banded cell wall pattern in metaxylem vessels (Supplementary Fig. 26). Together with the results of multiple knockout of FH genes, these results suggest that the activity to alter the pitted cell walls into banded cell walls is specific to FH11 and is not shared with other FH members that are expressed in xylem vessels.

https://doi.org/10.1038/s41467-025-56866-y

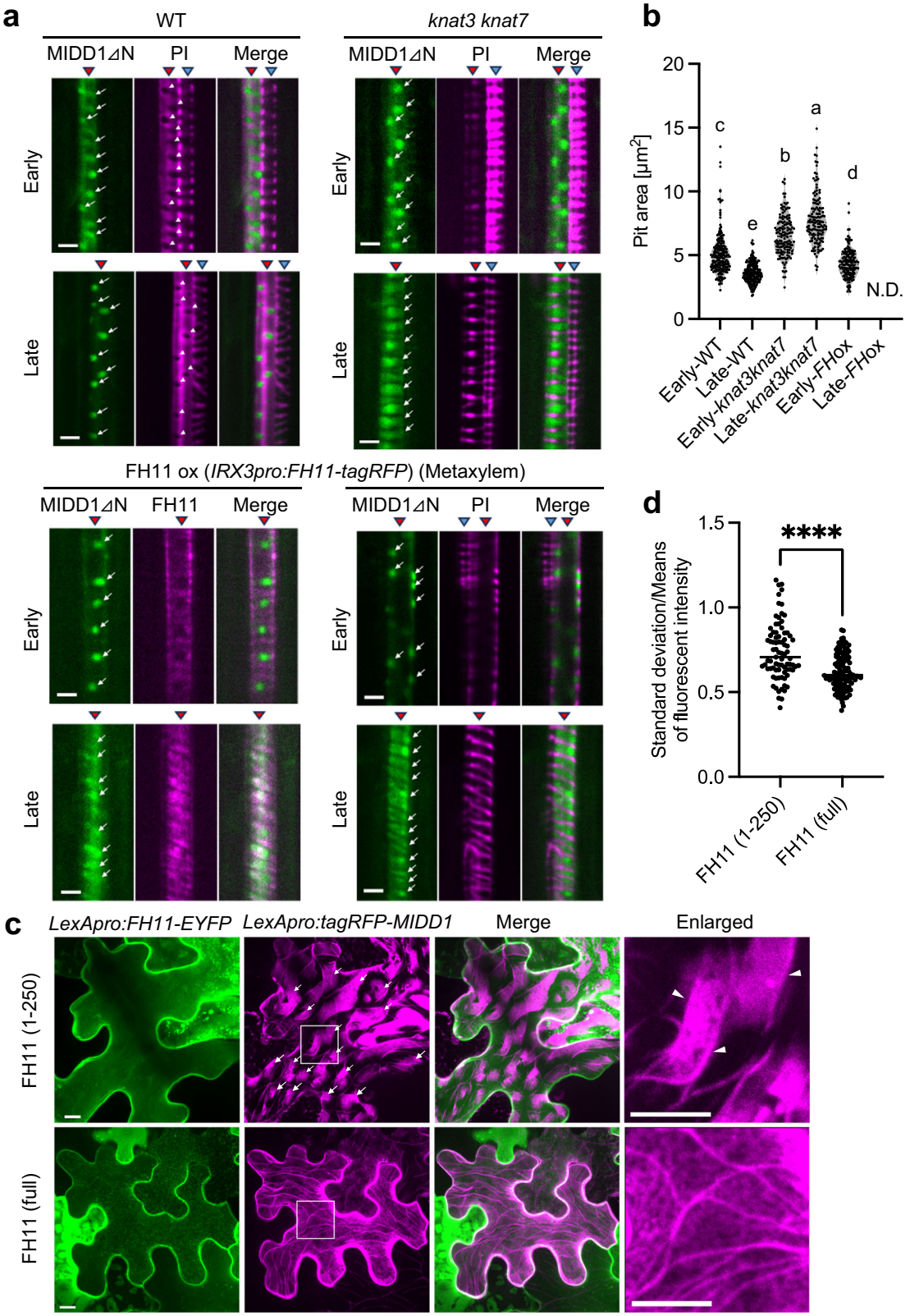

Discussion

KNAT7 acts both as a repressor and an activator of transcription in a tissue-dependent manner. In stem interfascicular fibers, KNAT7 represses genes involved in the biosynthesis of secondary cell wall components, including hemicellulose and monolignols[29,35,60]. By contrast, in seed coats, KNAT7 positively regulates genes involved in xylan biosynthesis in mucilage[35,60]. Our transcriptomic analysis of xylem cultures revealed that repression of *FH11* by *KNAT7* determined the secondary cell wall pattern in metaxylem vessels (Fig. 7). In the *knat7* mutant, *FH11* was upregulated in metaxylem cells, but not in protoxylem cells. The metaxylem-specific functions of KNAT7 probably result from its interactions with a variety of transcription factors, including OFP1, OFP4, BLH6, MYB75, and KNAT3[27,28,31,61], thus KNAT7 may interact with as-yet-unidentified transcription factor(s) to repress *FH11* in metaxylem cells.

Fig. 5 | FH11 expression results in diffuse localization of active ROPs in mature metaxylem vessels. a Localization of active ROPs (*MIDD1pro:MIDD1ΔN-GFP*) and cell walls (PI) in root metaxylem cells of wild-type (WT), *knat3 kant7*, and FH11-expressing plants (FH11 ox, *IRX3pro:FH11-tagRFP*) at the early and the late stages of metaxylem formation. White arrows indicate MIDD1ΔN-GFP fluorescence; white arrowheads indicate pit regions; red and blue arrowheads indicate metaxylem and protoxylem vessels, respectively. Scale bars = 5 μm. **b** Areas of MIDD1ΔN-GFP fluorescence spots were measured at the early and late stages of metaxylem vessel formation. MIDD1ΔN-GFP fluorescence areas could not be measured in FH11-expressing cells during the late stage due to diffusion (N.D.: not determined). Letters indicate significant differences between individual lines in one-way ANOVA with Dunnett's post hoc test; $n = 200$ (Early-WT), 190 (Late-WT), 140 (Early-*knat3 kant7*), 140 (Late-*knat3 knat7*) and 152 (Early-*FH*ox) pits; $P < 0.0001$. **c** Localization of tagRFP-MIDD1 (*LexApro:tagRFP-MIDD1)* and truncated FH11-EYFP (1-250, *LexApro:FH11 (1-250)-EYFP*) or full length FH11-EYFP (full, *LexApro:FH11-EYFP*) in epidermal cells of *N. benthamiana* co-expressing *LexApro:ROP11, LexApro:ROPGAP3, and LexApro:ROPGEF4PRONE*. The areas of white boxes are enlarged in the right panels. Arrows and arrowheads indicate the assembly of active ROPs and microtubules marked with MIDD1, respectively. Note that microtubules associate with the area occupied with active ROPs. Scale bars = 10 μm. See also Supplementary Figs. 20 and 21. **d** Standard deviation of the intensity of tagRFP-MIDD1. Dots represent individual data points in individual cells, while horizontal lines indicate the median value, $n = 81$ (FH11 (1-250)) and 119 (FH11 (full)) cells, $^{****}P < 0.0001$ (two-tailed Student's t test).

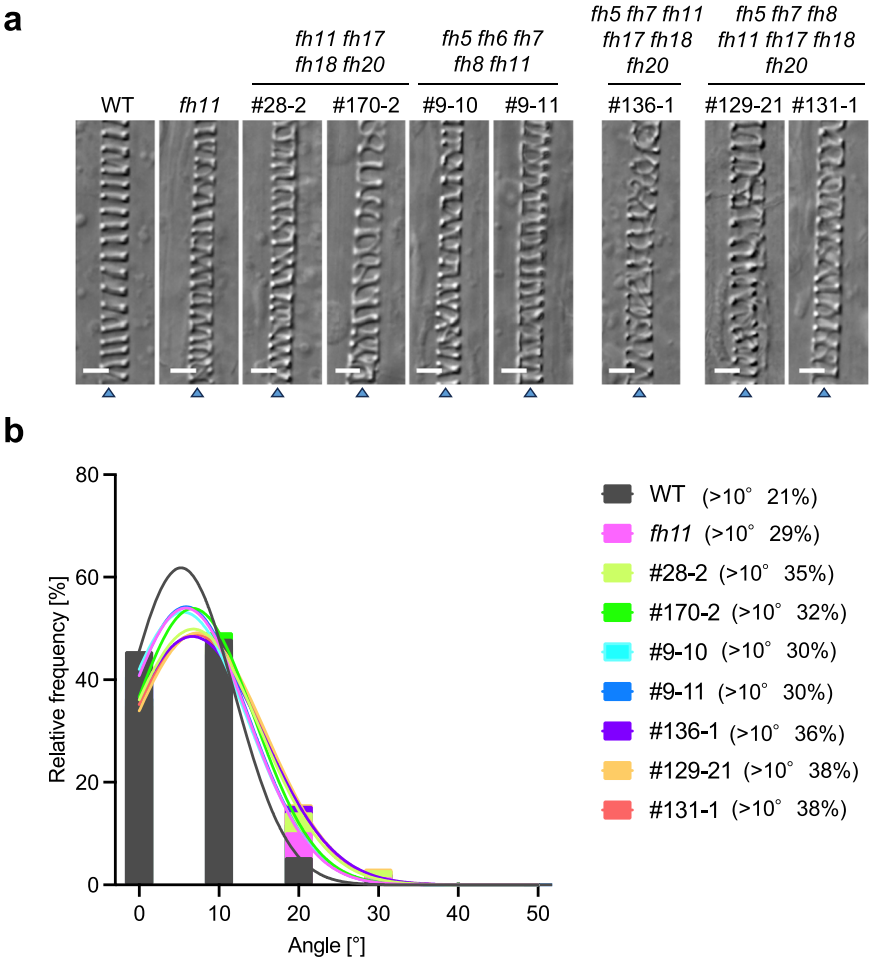

Fig. 6 | Knocking out *FH* genes disrupts cell wall band formation in protoxylem vessels. a Protoxylem vessel cells in the roots of *FH*-knockout mutants. Supplementary Fig. 23 contains detailed information about these mutants. Blue arrowheads indicate protoxylem vessels. Scale bars = 5 μm. **b** Angle of stripes in protoxylem vessel cells in the roots of *FH*-knockout mutants. The x-axis shows stripe angles in 10° increments and the y-axis the relative frequency of stripes within each increment. The values for individual lines are shown in the stacked bar graph. The individual segmented graphs are shown in Supplementary Fig. 24. The solid lines superimposed on the graph represent the theoretical curves of a Gaussian distribution. The proportions of stripes with angles > 10° for each line are shown on the right of the graph. $n = 829$ (WT), 883 (*fh11*), 870 (#28-2), 769 (#170-2), 1005 (#9-10), 909 (#9-11), 909 (#136-1), 788 (#129-21) and 698 (#131-1) stripes.

Loss of *KNAT7* led to misexpression of *FH11* in metaxylem vessels, which in turn induced the formation of banded rather than pitted cell walls (Fig. 7b). This was not due to a change in cell fate, as expression levels of HD-ZIPIII transcription factors were unchanged in *knat7*; furthermore, *KNAT7* is a target of VND6 and VND7, which directly induce the expression of genes involved in secondary cell wall biosynthesis and programmed cell death in xylem vessels[24,62]. Active ROPs were observed to localize on the plasma membrane in characteristic spots during the early stage of metaxylem differentiation in *knat7* mutants and in cells expressing exogenous *FH11* (Fig. 5a, b). Misexpression of FH11 caused dispersion of the active ROPs across the plasma membrane, resulting in a distribution resembling that in the protoxylem (Fig. 5c). FH11 thus induced the formation of banded cell walls by overriding the process of pit formation, not by changing the cell fate of the metaxylem.

In plants, FH family proteins have diverse roles in cell growth and morphogenesis[41,63,64], as well as in cytokinesis[65,66], symbiosis[67], plasmodesmata[68,69], and immune responses[70,71]. Our study revealed a

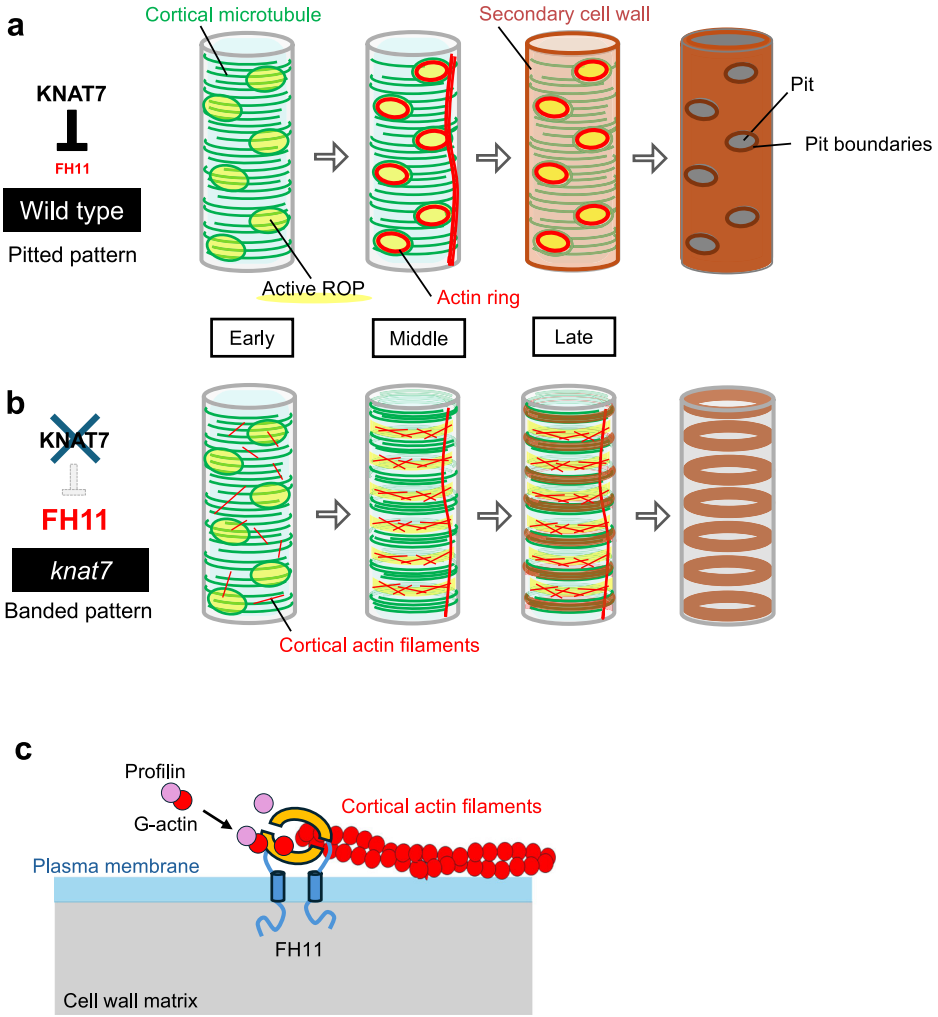

Fig. 7 | Schematic illustration of cell wall pattern formation in metaxylem vessels. a KNAT7 suppresses the expression of FH11 in the metaxylem vessels of wild-type plants, causing a pitted cell wall pattern to form. Secondary cell walls are deposited on microtubules. Active ROPs localize to spots on the plasma membrane where the microtubules are depolymerized through the MIDD1-Kinesin-13A pathway, ultimately leading to the formation of pits at points where the secondary cell wall is not deposited. Actin rings form around the spots of active ROPs and promote the deposition of secondary cell wall at pit boundaries. **b** In metaxylem vessels of *knat7*, misexpression of FH11 leads to the formation of a banded cell wall pattern. FH11 promotes the polymerization of cortical actin filaments, which disperses the ROP domains. **c** Dimeric FH11 on the plasma membrane promotes the polymerization of cortical actin filaments from monomeric actin bound to profilin. The extracellular domain of FH11 may interact with the cell wall matrix.

novel role for FH11. We found it induced a dramatic change in the secondary cell wall pattern and also in microtubule alignment and ROP distribution. These changes required actin polymerization by the FH1-FH2 domain of FH11, as well as transmembrane anchoring of the FH1-FH2 domain to the plasma membrane (Fig. 4; Supplementary Fig. 19). Given that microtubules guide the deposition of cell wall materials[5,72], the formation of bundled microtubules was probably the direct cause of banded cell wall formation in metaxylem vessels. Although the Arabidopsis FH proteins, FH4, FH13, FH14[73,74], and the mammalian formin, mDia1[75] bind to microtubules, FH11 did not localize to microtubules (Supplementary Fig. 15); thus it was unlikely that banded cell walls were induced by direct binding of FH11 to microtubular bundles.

Previously, we reported that cortical microtubules restrict the lateral diffusion of ROPs at the plasma membrane[8,12], and that active ROPs promote the depletion of microtubules through the MIDD1-Kinesin-13A pathway[7,9,10]. We observed in this study that active ROPs dispersed from the spots to the regions between the nascent cell wall bands in *knat7* and *FH11*-expressing metaxylem cells (Fig. 5a, b). Ectopic expression of FH11 reduced the EYFP-TUB6 signal and the density of EB1 at the cell cortex (Supplementary Figs. 14d, 16), thus plasma membrane-associated actin filaments induced by FH11 may have inhibited the dynamics of cortical microtubules or the microtubule-plasma membrane interaction. The mutually exclusive localization of FH11 and cortical microtubules (Supplementary Figs. 7, 10c) also suggests the possible inhibitory effects of FH11-induced actin filaments on microtubules. An in vitro study also showed that the actin filament network inhibits microtubule growth[76]. This would enable active ROPs to diffuse, resulting in the formation of larger microtubule-depleted areas with narrow bands of microtubules between them. This scenario is supported by our observation that FH11 inhibited the ectopically induced local accumulation of active ROPs, which was segmented by the cortical microtubules, on the plasma membrane in *N. benthamiana* leaves (Fig. 5c; Supplementary Figs. 20, 21). FH1, another FH protein associated with the plasma membrane[77], affects microtubule dynamics in cotyledon pavement cells[78], which also supports this hypothesis.

Another possibility is that FH11 affected the active ROP localization by regulating ROPGEF. In pollen tubes, actin polymerization promotes ROPGEF activation through the receptor-like kinase, PRK2[79,80]. Similarly, in xylem vessels, actin filaments polymerized by

FH11 may promote ROPGEFs at pits through yet-to-be-identified factors, thereby expanding the area of active ROPs from the pits. In any case, detailed observations of these regulatory elements, especially during the early stage of xylem differentiation, are desirable to determine the mechanism by which FH11 alters the cell wall pattern.

The N-terminal region of FH11, which includes the extracellular domain and the transmembrane domain, was essential for the induction of banded cell walls in metaxylem vessels (Fig. 7c). Replacement of this region with RCI2A/LTI6a confirmed that the transmembrane domain was required for FH11 activity, whereas the extracellular domain was probably dispensable (Fig. 4c-e). FH1 from Arabidopsis and SYMBIOTIC FORMIN 1 (SYFO1) from *Medicago truncatula* also localize to the plasma membrane[67,77,81]. These two proteins are immobilized by their N-terminal domains, which contain the Ser-Pro-Pro-Pro EXTENSIN-like motif thought to interact with cell wall pectins[82]. FH11 lacks an EXTENSIN-like motif, however, suggesting its relationship with the extracellular space differs from that of FH1 and SYFO1. Given that the transmembrane and the FH1-FH2 domains of FH11 were compatible with those of other proteins in our swapping analysis (Fig. 4c-e), the distinct functions of FH11 are likely to depend on the nature of its extracellular domain. The remodeling of cortical microtubules and cell wall patterns are important events in various processes, including cell differentiation[83], mechanical responses[84,85], immune responses[86,87], and environmental responses[88]. Our study implies that actin polymerization at the plasma membrane could be a potential target for remodeling of microtubules and cell wall patterns within cells. Publicly available expression data[89,90] show that FH11 is expressed in embryos, stomatal lineages, and flowers. It will be worth investigating how FH11 contributes to cell wall patterning in these tissues.

The overexpression of other FHs that are expressed in xylem vessels, FH5, FH6, FH7, FH17, FH18, and FH20 did not induce the banded cell wall pattern. These FHs showed various localization patterns in xylem vessel cells, probably due to their different N-terminal sequences (Supplementary Figs. 26-28). It is possible that they have highly diversified functions even in the same tissues. Further elucidation of the functions of these FHs will be an important direction for future research.

The effect of actin polymerization on cell wall patterning revealed in the present study could lead to the development of novel strategies for manipulating plant cell walls for agricultural applications. Drought stress or ABA treatment activates VND7, thus switching metaxylem to protoxylem[91]. The banded cell walls of protoxylem allow more efficient lateral water transport than do the pitted cell walls of metaxylem[91,92]. The formation of protoxylem under drought conditions is thus likely to enhance recovery from embolism, reducing the risk of mortality from disrupted water transport along vascular bundles[92]. The transformation of pitted into banded cell wall pattern in metaxylem vessels had no noticeable impact on plant growth under normal growth conditions (Supplementary Fig. 5). The KNAT7-FH11 module could therefore be used as a tool to enhance plant drought tolerance by rapidly inducing banded cell walls without changing cell fate in response to drought stress.

Methods

Plant materials and growth conditions

Arabidopsis thaliana plants utilized in this study were all in the Columbia-0 (Col-0) background. T-DNA insertion lines *fh11* (GABI-348C07 (CS750570)), *knat7* (SALK_002098 C) and *knat3* (SALK_136464) were obtained from ABRC. The #77-41 was generated by EMS mutagenesis in this study. *gef4 gef7* and *gap3 gap4* mutants have been reported previously[11]. Arabidopsis plants were transformed by the floral dip method using *Agrobacterium tumefaciens* (MP90). Multiple knockout plants of formin genes were generated by CRISPR/Cas9 genome editing system in this study.

Seedlings were grown on 1/2 MS agar medium containing 0.2% sucrose at 22˚C under constant light. Hypocotyl of etiolated seedlings were grown under the light shielding condition for 5 days. For the expression of estrogen-inducible genes, 5-day-old seedlings or etiolated seedlings were transferred into 1/2 MS agar medium containing 2 μM β-estradiol and incubated for 24 h. Arabidopsis suspension cultured cells were cultured at 22°C with suspension at 120 rpm and transformed by co-cultured with *Agrobacterium tumefaciens* (MP90)[9]. On the 8th day after transformation, the cells were treated with 2 μM β-estradiol, and 24 h later, they were labeled with 3.2 μM FM4-64 (Thermo Fisher Scientific) just before observation. Transient expression in *N. benthamiana* was performed by the infiltration of *Agrobacterium tumefaciens* (MP90) suspended in infiltration buffer (10 mM MES (pH 5.7), 10 mM $MgCl_2$, 50 mg/L acetosyringone)[8]. Samples of leaves grown for 2 days after infiltration were floated in water including 2 μM β-estradiol and observed after 1 or 2 days.

Genome sequencing analysis

The mutation in the genome of #77-41 generated by EMS mutagenesis was identified by next-generation sequencing (NGS) analysis. Illumina HiSeq 2000 paired-end sequencing was performed by the BGI (Shenzhen, China). Low-quality reads and adapter sequences were removed using Tagdust[93] and Sickle (https://github.com/najoshi/sickle). The trimmed reads were mapped to the Arabidopsis TAIR10 reference genome (https://www.arabidopsis.org/) using Bowtie2[94] and SNPs of the genome were detected using SAMtools[95].

Plasmid construction

Primers used in this study were listed in Supplementary Table 3. The coding sequences of *KNAT7*, *FH11* and truncated *FH11* were amplified from the Arabidopsis genome by PCR with appropriate primers and cloned into *pEntr/D-TOPO* cloning vector (Thermo scientific). For the construction of swapped *FH11*, *FH11* CDS was amplified from the *Arabidopsis* cDNA by PCR. After cloning into *pEntr/D-TOPO*, insertion of mutations and swapping were performed by using PCR and In-Fusion HD Cloning kit (Takara) with appropriate primers. The templates of *DIAPH1*, *RCI2A* and *ARA6* were obtained from Addgene (Cat. #54156), subcloned RCI2A[96] and *Arabidopsis* cDNA, respectively. Domains of *LAMP1*, *RLK* and palmitoylation signal were amplified by inverse PCR with appropriate primers. The *KNAT7* promoter (2 kbp), FH11 promoter (2.5 kbp) and *IRX3* promoter (1.5 kbp) were inserted into the *NotI* site upstream of individual clones of the *pEntr/D-TOPO* by In-Fusion HD Cloning kit. To construct *IRX3pro:FHs*, genomic sequences of *FH5, FH6, FH7, FH17, FH18*, and *FH20* were amplified by PCR and inserted into *pEntr/D-TOPO* cloning vector with *IRX3* (1.5 kbp) promoter. Those clones were fused with GFP or tagRFP, and cloned into pER8 vector[8,42], *pUNC-YFP-Dest* and *pUBC-RFP-Dest* with *UBQ10* promoter[97], and *pGWB640, pGWB540, pGWB659, pGWB501, pGWB402* and *pGWB404*[98] by using LR Clonase Mix II (Thermo Fisher Scientific). *PRF1* fused with *LPETG-His8*-tag and *FH1-FH2* fused with *GFP*-tag were cloned in a *pCold* vector (Takara) and a *pEU* vector (Cell Free Science Co., Ltd.), respectively. The expression vector containing the *LexApro:ROP11, LexApro:ROPGAP3*, and *LexApro:ROPGEF4PRONE* cassettes and the *LexApro:tagRFP-MIDD1* vector were described previously[8]. To make the *pUBQ10:mTurquoise2-TUB6* vector, the coding sequence of *TUB6* was fused with the 1.2 kbp *UBQ10* promoter sequence and the *mTurquoise2* coding sequence in the *pEntr/D-TOPO* vector, followed by the recombination with the *pGWB501* vector by using LR Clonase Mix II. To construct plasmids for the transient effector-reporter assay, cDNA of *KNAT7* and 1 kbp- or 2 kbp-length promoter sequences of *FH11* were cloned into the *pDEST35SHSP*[99] and *pTATA_LUC_HSP* vectors[39], respectively.

Transient effector-reporter analysis

Transient luciferase reporter analysis was performed using protoplasts isolated from Arabidopsis rosette leaves by the Tape-Arabidopsis Sandwich method[100]. The outer skin on the underside of the rosette

leaves was removed using cellophane tape and treated with an enzyme solution (1% cellulase onozuka R10 (Yakult), 0.25% macerozyme R10 (Yakult), 0.4 M mannitol, 20 mM MES (pH 5.7), 20 mM KCl, 10 mM $CaCl_2$ and 5 mM 2-mercaptoethanol). Isolated protoplasts were washed with W5 buffer (150 mM NaCl, 125 mM $CaCl_2$, 5 mM KCl, and 2 mM MES (pH 5.7)) and resuspended in MMg solution (0.4 M mannitol, 15 mM $MgCl_2$, and 4 mM MES (pH 5.7)). Firefly luciferase driven by the *FH11* promoters with TATA box and omega element was employed as a reporter. *KNAT7* CDS and *VAMP722* under the control of *35S* promoter with omega element were employed as an effector and control, respectively. As the internal reference, a modified *Renilla luciferase* (*hRLUC*, Promega Inc.) gene drive by the *35S* promoter was used to normalize the data. *pDEST35SHSP* plasmid was used as the buffer plasmid. Protoplast suspension were mixed with 300 ng of the reporter plasmid, 100 ng of the effector plasmid, 100 ng of the buffer plasmid, and 10 ng of the reference plasmid and transformed in transformation solution (40% polyethylene glycol, 0.2 M mannitol, and 0.1 M $CaCl_2$) and incubated for 10 min in a 96 well plate. After washing the transformed protoplasts with W5 buffer, they were incubated at 22 °C for 18 h in the dark. The luminescent intensity of luciferin was detected by plate reader (INFINITE F200, TECAN).

Quantitative RT-PCR

For extraction of RNA from the differentiating cells, 5-day-old Arabidopsis seedlings were ectopically differentiated into metaxylem vessels by cultured in MS liquid medium supplemented with 1 mg/L kinetin, 0.1 mg/L 2,4-D, and 10 μM bikinin[36,37]. Seven days after induction, total RNA was extracted by RNeasy Plant Mini kit (Qiagen). Purified RNA was reverse transcribed using oligo (dT) 20 primers and SuperScript IV reverse transcriptase (Thermo Fisher Scientific). Quantitative RT-PCR was performed with FastStart Essential DNA Green Master (Roche Diagnostics) by using LightCycler 96 and the software (Roche Diagnostics). The expression level of *UBQ10* was used as internal control for normalizing. Used primers and analyzed genes were listed in Supplementary Table 4.

Protein preparation

G-actin was prepared from a rabbit skeletal muscle acetone powder[101] and G-actin was purified by gel-filtration chromatography on Sephacryl S-300 in G-buffer (2 mM Tris-HCl (pH 8.0), 0.2 mM ATP, 0.2 mM $CaCl_2$, 0.5 mM DTT) at 4 °C. Purified unlabeled G-actin was lyophilized after adding sucrose to 0.1 M and preserved as actin sucrose powder. This actin sucrose powder was diluted in G-buffer. The G-actin was polymerized in polymerization buffer (10 mM HEPES (pH 7.5), 100 mM KCl, 5 mM $MgCl_2$, 1 mM EGTA, 1 mM ATP). The actin filaments were then dissolved in polymerization buffer supplemented with 1 mM ATP and incubated with ATTO565-NHS (AD565-31, ATTO-TEC) at a dye:actin molar ration of 5:1 at 37 °C for 30 min. Unreacted dye was removed by performing a polymerization-depolymerization cycle[76]. The labeled G-actin was mixed with unlabeled G-actin at 10% in a molar ratio.

The PRF1-LPETG-His8-tag in a *pColdI* vector was expressed in *Escherichia coli* BL21 (DE3) cells. The expression procedure was performed following the general *pCold* vector manual (Takara). The protein was purified using Ni-NTA agarose resin (QIAGEN) and eluted with an elution buffer (20 mM Tris-HCl (pH8.0), 150 mM NaCl, 500 mM Imidazole). The purified protein was filtrated using Amicon Ultra 3k and buffer was replaced with a storage buffer (20 mM Tris-HCl (pH 8.0), 1 mM DTT, 1 mM EDTA).

FH1-FH2-GFP was purified by using cell-free protein synthesis system with the WEPRO7420 Expression kit (Cell Free Science Co., Ltd.) following the manufacturer's instructions.

In vitro actin polymerization assay

A flow cell was assembled on a glass substrate with a cover slip modified with polyethylene glycol (PEG)[102] and double-sided tape as the spacer. 5 μl of the 1% BSA in 1×HKEM buffer (10 mM HEPES (pH 7.4), 50 mM KCl, 5 mM $MgCl_2$, 1 mM EGTA) was perfused into the flow cell. 7 μL of actin polymerization mix (1×HKEM buffer supplemented with 10 mM DTT, 3 mM ATP, 0.33× G-buffer, 9 mg/mL D-glucose, 100 U/mL glucose oxidase, and 200 U/mL catalase, 0.33 % methylcellulose (cP4000)) including PRF1 with or without FH1-FH2-GFP was applied to the flow cell. All in vitro experiments were carried out at 25 °C.

Microscopy

DIC imaging of xylem vessels were obtained using an upright microscope (BX-53, Olympus) equipped with differential interference contrast unit, a digital microscope camera (DP73, Olympus) and a UPLANSAPO 40 × /0.95 NA objective (Olympus). Images were acquired using cellSens software (Olympus). Root tissues were cleared by clear solution (100 g Chloral Hydrate dissolved in 25 mL H_2O and 10 mL Glycerol).

For confocal imaging, we used an inverted microscope (IX83-ZDC, Olympus) equipped with a spinning disk confocal scanning unit (CSU-W1, Yokogawa), two sCMOS cameras (ORCA-Fusion, Hamamatsu Photonics), a UPLANSAPO 60 × /1.20 NA water-immersion objective (Olympus), and laser lines set at 445, 488, 514, and 561-nm. Images were acquired using MetaMorph software (Molecular Devices). Before observation, the Arabidopsis cultured cells and *N. benthamiana* leaves were transferred to a glass-bottom dish (Matsunami). Arabidopsis seedlings and roots were held in a slide glass covered with a coverslip (Matsunami). For propidium iodide (PI) staining, roots and hypocotyl cells were stained with 1 μg/mL and 10 μg/mL PI (Thermo Fisher Scientific) in water, respectively. To analyze EB1 dynamics, images were acquired every 3 s for 3 min.

For VA-TIRF microscopy of Arabidopsis seedlings in Supplementary Fig. 11a, b, we used an inverted microscope (Ti, Nikon) equipped with total internal reflection fluorescence (TIRF), EMCCD camera (iXon Ultra, Andor), an Apo TIRF 100 × /1.49 NA oil-immersion objective (Nikon), and a 488 nm laser. To analyze actin filament dynamics, images were acquired every 1 s for 1 min. For VA-TIRF microscopy in Supplementary Fig. 11c, we used an inverted TIRF microscope (Ti2-E, Nikon) equipped with 405, 488, 561, and 640 nm lasers, an EM-CCD camera (ImagEM, Hamamatsu photonics), and an Apo TIRF 100 × /1.49 NA oil-immersion objective (Nikon). Images were acquired using NIS-Elements software (Nikon).

For TIRF microscopy of in vitro actin polymerization analysis in Supplementary Fig. 17, we used an inverted microscope (Ti2-E, Nikon) equipped with ReLIEF illumination system (Optoline Inc.), EM-CCD camera (iXonEM + , Andor), a 60× Plan Apo TIRF (N.A. = 1.49) oil-immersion objective (Nikon), appropriate filter sets (originally designed filter cube: 50/50 mirror (Chroma), BA606/55; FITC filter cube: EX480/30, DM505, BA535/45 (Nikon)) and a laser light source (Skyler, Cobolt). Images were acquired using NIS elements BR (Nikon).

To obtain volume rendering and omni-directional images of protoxylem vessels (Supplementary Fig. 25), roots were stained by basic fuchsin staining after ClearSee treatment[103]. The stained roots were observed under an Olympus FV3000 inverted confocal microscope (Olympus) equipped with an UPLAN 60× water-immersion objective (N.A. = 1.2), and a laser line set to 561 nm. Images were acquired using FV-OSR software (Olympus). Three dimensional images were generated from z-stack images using Imaris software (Bitplane Company). To obtain omni-directional images, z-stack images were processed and converted into 360° two-dimensional images using an ImageJ plug-in developed in the previous studies[9,11].

Quantification of the banded cell wall pattern

To evaluate the type of cell wall patterns, the DIC images of metaxylem vessels were normalized and converted to the 8 bit gray scale. Subsequently, the 500 × 35 pixels (54.6 × 3.83 μm) areas of the metaxylem vessels were segmented. Using the newly developed Image J plugin

(SDLT_Ratio: the equations of the plugin are show below), the aspect ratio (AR) between the mean standard deviation (SD) of each longitudinal (column) pixel value (S_i, $0 \leqq i \leqq 34$) and the mean SD of each transverse (row) pixel value (S_j, $0 \leqq j \leqq 499$) of the segmented area were calculated. In the equations, J and I indicate the number of longitudinal and transverse pixels, respectively ($J = 500$, $I = 35$). $x_i y_j$ indicates intensity value of pixel (i, j). In this method, the typical scores of the banded and pitted cell walls are over 1.0 and around 0.5 - 0.8, respectively.

$$S_i = \sqrt{\frac{\sum_j \left(x_i y_j - \overline{x_i y}\right)^2}{J}}$$

$$S_j = \sqrt{\frac{\sum_i \left(x_i y_j - \overline{x y_j}\right)^2}{I}}$$

$$AR = \bar{S}_i / \bar{S}_j$$

The source code is provided in Supplementary Data 1.

RNAseq of cultured hypocotyls and cotyledons

Induction of ectopic xylem cells in cultured hypocotyls and cotyledons were conducted in MS liquid medium supplemented with 1.25 mg/L 2,4-D, 0.25 mg/L kinetin, and 10 μM bikinin, and in MS liquid medium supplemented with 1 mg/L kinetin, 0.1 mg/L 2,4-D, and 10 μM bikinin, respectively[13,36,37]. The total RNA of the cultured hypocotyls at 6 days after the onset of the culture and cotyledons at 4 days after the onset of the culture was extracted by RNeasy Plant Mini kit (Qiagen). The total RNA was extracted from the three sets of independent biological samples.

mRNA-seq libraries were constructed from 600 ng of total RNA using the KAPA mRNA HyperPrep Kit (Kapa Biosystems). Three independent biological replicates were analyzed for each genotype. The resulting libraries were 50 bases single-end sequenced by the HiSeq4000 sequencer (Illumina) in Vincent J. Coates Genomics Sequencing Laboratory at UC Berkeley.

Quality-filtered and adapter-trimmed reads were mapped on the Arabidopsis TAIR10 genome using STAR aligner[104] with –outFilterType BySJout – alignSJoverhangMin 8 – alignSJDBoverhangMin 1 – quantMode GeneCounts parameters. The resulting per-gene counts were used for downstream analysis.

Differentially expressed genes (DEGs) were identified in R using the R package edgeR[105], treating biological triplicates as paired samples.

Quantification of fluorescent intensity of *FH11*

The fluorescent intensity of *FH11pro:FH11-EYFP* in xylem vessels or *LexApro:FH11-tagRFP* in root epidermal cells were quantified by using ImageJ (https://imagej.nih.gov/ij/). The mean value of the fluorescent intensity within a 3.255 μm x 11.935 μm area in xylem vessels or 3.8 ×3.8 μm area in root epidermal cells of slice images of root xylem vessel cells was subtracted from the mean value of the background fluorescent intensity in each cell.

Quantification of density and skewness of cytoskeleton

Quantification of density and skewness of cytoskeleton was performed by using ImageJ. Slice images of root or hypocotyl epidermal cells or stack images of *N. benthamiana* leaf epidermal cells were analyzed. The focal plane in individual images was manually selected. Skewness which reflects bundling index calculated by pixel intensity distribution was measured by the Skewness function of ImageJ. For determine the density, filaments of cytoskeleton were extracted by using the Ridge Detection plug-in in ImageJ (https://imagej.net/plugins/ridge-detection) and the density was obtained from the generated binary images by the Area function of ImageJ. The histogram of fluorescent intensity was quantified by the plot profile function of ImageJ. Graphs were drawn using GraphPad Prism 9 software (GraphPad Software).

Analysis of the localization pattern of active ROPs in leaf epidermal cells of *N. benthamiana*

Confocal stack images of *N. benthamiana* leaf epidermal cells were processed into maximum-intensity projections. Each cell area in the projected images was manually selected and the standard deviation and means of the fluorescent intensity of tagRFP-MIDD1 in each cell area were quantified by using Image J functions.

Genome editing by the CRISPR/Cas9 system

Target sequences for the CRISPR/Cas9 were listed in Supplementary Table 5. To induce the multiple mutations, the gRNA cassettes containing the target sequences were tandemly cloned into the pKAMA-ITACHI *pKI1.1 R* vector[106] or *pDe*[107] based Cas9 vector. After the homo mutation lines were obtained, the CRISPR/Cas9 cassette were eliminated by using the Fast-Red fluorescent marker.

Quantification of protoxylem vessel angle

The binary images of the cell wall bands of protoxylem vessels were obtained semi-automatically from the DIC images using an ImageJ plug-in developed in the previous studies[10]. Individual angle of each cell wall was determined by using the fit ellipse of the analyze particle function. A value of width of 3.28 μm or greater was analyzed and the angular displacements were transformed to be positive value.

Quantification of dynamics of actin filaments and EB1

To analyze actin filament dynamics, a 30 s time-lapse sequence of in-focus images was acquired. The Pearson's correlation co-efficient (r) between the first frame and each time frame of the time-lapse sequence in 4 x 20 μm^2 ROIs was calculated using the coloc-2 plugin of Fiji software. To quantify the EB1 density, the number of EB1 in the manually selected region of z-stack images was counted by Analyze particles function of ImageJ. The EB1 velocity was calculated using the Manual Tracking plug-in of the Fiji software. We defined the average velocity of EB1 as the mean speed over 3 seconds for particles that could be tracked for over 30 s.

Reporting summary

Further information on research design is available in the Nature Portfolio Reporting Summary linked to this article.

Data availability

The data supporting the findings of this study are available within the article, the Supplementary Information files, and the Source Data files accompanying this article. The high-throughput sequencing data obtained in this study is available at NCBI database with the accession number GSE286145. Source data are provided with this paper.

Code availability

The code used in this study for quantification of the banded cell wall pattern is available in Supplementary Data 1 as a.txt file, which accompanies this article.

References

1. Meents, M. J., Watanabe, Y. & Samuels, A. L. The cell biology of secondary cell wall biosynthesis. *Ann Bot*. **121**, 1107–1125 (2018).
2. Zhong, R. Q., Cui, D. T. & Ye, Z. H. Secondary cell wall biosynthesis. *New Phytologist* **221**, 1703–1723 (2019).

3. Oda, Y. & Fukuda, H. Secondary cell wall patterning during xylem differentiation. *Curr. Opin. Plant Biol.* **15**, 38–44 (2012).
4. Xu, H. et al. Secondary cell wall patterning-connecting the dots, pits and helices. *Open Biol*. **12**, 210208 (2022).
5. Watanabe, Y. et al. Visualization of cellulose synthases in Arabidopsis secondary cell walls. *Science* **350**, 198–203 (2015).
6. Paredez, A. R., Somerville, C. R. & Ehrhardt, D. W. Visualization of cellulose synthase demonstrates functional association with microtubules. *Science* **312**, 1491–1495 (2006).
7. Oda, Y. & Fukuda, H. Rho of plant GTPase signaling regulates the behavior of Arabidopsis kinesin-13A to establish secondary cell wall patterns. *Plant Cell* **25**, 4439–4450 (2013).
8. Oda, Y. & Fukuda, H. Initiation of cell wall pattern by a Rho- and microtubule-driven symmetry breaking. *Science* **337**, 1333–1336 (2012).
9. Oda, Y., Iida, Y., Kondo, Y. & Fukuda, H. Wood cell-wall structure requires local 2D-microtubule disassembly by a novel plasma membrane-anchored protein. *Curr Biol*. **20**, 1197–1202 (2010).
10. Higa, T. et al. Microtubule-associated phase separation of MIDD1 tunes cell wall spacing in xylem vessels in Arabidopsis thaliana. *Nature plants* **10**, 100–117 (2024).
11. Nagashima, Y. et al. A Rho-based reaction-diffusion system governs cell wall patterning in xylem vessels. *Sci. Rep.* **8**, 11542 (2018).
12. Sugiyama, Y., Wakazaki, M., Toyooka, K., Fukuda, H. & Oda, Y. A novel plasma membrane-anchored protein regulates xylem cell-wall deposition through microtubule-dependent lateral inhibition of rho gtpase domains. *Curr. Biol.* **27**, 2522–2528.e2524 (2017).
13. Sasaki, T., Fukuda, H. & Oda, Y. Cortical microtubule disordering1 is required for secondary cell wall patterning in xylem vessels. *Plant Cell* **29**, 3123–3139 (2017).
14. Sasaki, T. et al. Confined-microtubule assembly shapes three-dimensional cell wall structures in xylem vessels. *Nature communications* **14**, 6987 (2023).
15. Pesquet, E., Korolev, A. V., Calder, G. & Lloyd, C. W. The microtubule-associated protein AtMAP70-5 regulates secondary wall patterning in Arabidopsis wood cells. *Curr. Biol.* **20**, 744–749 (2010).
16. Smertenko, T. et al. MAP20 functions in metaxylem pit development and contributes to drought recovery. *New Phytologist* **227**, 1681–1695 (2020).
17. Schneider, R. et al. Long-term single-cell imaging and simulations of microtubules reveal principles behind wall patterning during proto-xylem development. *Nature communications* **12**, 669 (2021).
18. Jacobs, B., Schneider, R., Molenaar, J., Filion, L. & Deinum, E. E. Microtubule nucleation complex behavior is critical for cortical array homogeneity and xylem wall patterning. *Proc. Natl. Acad. Sci. Usa.* **119**, e2203900119 (2022).
19. Kobayashi, H., Fukuda, H. & Shibaoka, H. Reorganization of actin-filaments associated with the differentiation of tracheary elements in zinnia mesophyll-cells. *Protoplasma* **138**, 69–71 (1987).
20. Wightman, R. & Turner, S. R. The roles of the cytoskeleton during cellulose deposition at the secondary cell wall. *Plant J*. **54**, 794–805 (2008).
21. Sugiyama, Y. et al. A Rho-actin signaling pathway shapes cell wall boundaries in Arabidopsis xylem vessels. *Nat. Commun.* **10**, 468 (2019).
22. Carlsbecker, A. et al. Cell signalling by microRNA165/6 directs gene dose-dependent root cell fate. *Nature* **465**, 316–321 (2010).
23. Miyashima, S., Koi, S., Hashimoto, T. & Nakajima, K. Non-cell-autonomous microRNA165 acts in a dose-dependent manner to regulate multiple differentiation status in the Arabidopsis root. *Development* **138**, 2303–2313 (2011).
24. Kubo, M. et al. Transcription switches for protoxylem and metaxylem vessel formation. *Genes Dev*. **19**, 1855–1860 (2005).
25. Yamaguchi, M., Kubo, M., Fukuda, H. & Demura, T. Vascular-related NAC-DOMAIN7 is involved in the differentiation of all types of xylem vessels in Arabidopsis roots and shoots. *Plant J*. **55**, 652–664 (2008).
26. Zhong, R., Lee, C., Zhou, J., McCarthy, R. L. & Ye, Z. H. A battery of transcription factors involved in the regulation of secondary cell wall biosynthesis in Arabidopsis. *Plant Cell* **20**, 2763–2782 (2008).
27. Li, E., Wang, S., Liu, Y., Chen, J. G. & Douglas, C. J. OVATE FAMILY PROTEIN4 (OFP4) interaction with KNAT7 regulates secondary cell wall formation in Arabidopsis thaliana. *Plant J.* **67**, 328–341 (2011).
28. Liu, Y. Y. et al. Bel1-like homeodomain6 and knotted arabidopsis thaliana7 interact and regulate secondary cell wall formation via repression of REVOLUTA. *Plant Cell* **26**, 4843–4861 (2014).
29. Li, E. Y. et al. The Class II KNOX gene KNAT7 negatively regulates secondary wall formation in Arabidopsis and is functionally conserved in Populus. *New Phytologist* **194**, 102–115 (2012).
30. Wang, S. M. et al. The Class II KNOX genes and work cooperatively to influence deposition of secondary cell walls that provide mechanical support to Arabidopsis stems. *Plant J*. **101**, 293–309 (2020).
31. Qin, W. Q. et al. The class II KNOX transcription factors KNAT3 and KNAT7 synergistically regulate monolignol biosynthesis in Arabidopsis. *J. Exp. Bot.* **71**, 5469–5483 (2020).
32. Higashida, C. et al. Actin polymerization-driven molecular movement of mDia1 in living cells. *Science* **303**, 2007–2010 (2004).
33. Pruyne, D. et al. Role of formins in actin assembly: nucleation and barbed-end association. *Science* **297**, 612–615 (2002).
34. Romero, S. et al. How ATP hydrolysis controls filament assembly from profilin-actin: implication for formin processivity. *J. Biol. Chem.* **282**, 8435–8445 (2007).
35. Wang, Y. et al. KNAT7 regulates xylan biosynthesis in Arabidopsis seed-coat mucilage. *J. Exp. Bot.* **71**, 4125–4139 (2020).
36. Sasaki, T. & Oda, Y. Imaging of developing metaxylem vessel elements in cultured hypocotyls. *Methods Mol. Biol*. **1992**, 351–358 (2019).
37. Kondo, Y., Fujita, T., Sugiyama, M. & Fukuda, H. A novel system for xylem cell differentiation in Arabidopsis thaliana. *Molecular plant* **8**, 612–621 (2015).
38. Gardiner, J. C. Control of cellulose synthase complex localization in developing xylem. *Plant Cell Online* **15**, 1740–1748 (2003).
39. Yoshida, K. et al. Engineering the Oryza sativa cell wall with rice NAC transcription factors regulating secondary wall formation. *Front. Plant Sci.* **4**, 383 (2013).
40. Brown, D. M., Zeef, L. A., Ellis, J., Goodacre, R. & Turner, S. R. Identification of novel genes in Arabidopsis involved in secondary cell wall formation using expression profiling and reverse genetics. *Plant Cell* **17**, 2281–2295 (2005).
41. Blanchoin, L. & Staiger, C. J. Plant formins: Diverse isoforms and unique molecular mechanism. *Bba-Mol Cell Res*. **1803**, 201–206 (2010).
42. Zuo, J., Niu, Q. W. & Chua, N. H. Technical advance: An estrogen receptor-based transactivator XVE mediates highly inducible gene expression in transgenic plants. *Plant J*. **24**, 265–273 (2000).
43. Vidali, L., Augustine, R. C., Kleinman, K. P. & Bezanilla, M. Profilin is essential for tip growth in the moss Physcomitrella patens. *Plant Cell* **19**, 3705–3722 (2007).
44. Chaudhry, F., Guérin, C., von Witsch, M., Blanchoin, L. & Staiger, C. J. Identification of Arabidopsis cyclase-associated protein 1 as the first nucleotide exchange factor for plant actin. *Mol Biol Cell* **18**, 3002–3014 (2007).
45. Blanchoin, L., Boujemaa-Paterski, R., Sykes, C. & Plastino, J. Actin dynamics, architecture, and mechanics in cell motility. *Physiol Rev*. **94**, 235–263 (2014).

46. Pollard, T. D., Blanchoin, L. & Mullins, R. D. Molecular mechanisms controlling actin filament dynamics in nonmuscle cells. *Annu Rev Biophys Biomol Struct*. **29**, 545–576 (2000).
47. Funk, J. et al. Profilin and formin constitute a pacemaker system for robust actin filament growth. *eLife* **8**, e50963 (2019).
48. Romero, S. et al. Formin is a processive motor that requires profilin to accelerate actin assembly and associated ATP hydrolysis. *Cell* **119**, 419–429 (2004).
49. Zhang, S. et al. A processive arabidopsis formin modulates actin filament dynamics in association with profilin. *Molecular plant* **9**, 900–910 (2016).
50. Xu, Y. et al. Crystal structures of a Formin Homology-2 domain reveal a tethered dimer architecture. *Cell* **116**, 711–723 (2004).
51. Li, F. & Higgs, H. N. The mouse formin mDia1 is a potent actin nucleation factor regulated by autoinhibition. *Curr. Biol.* **13**, 1335–1340 (2003).
52. Watanabe, N., Kato, T., Fujita, A., Ishizaki, T. & Narumiya, S. Cooperation between mDia1 and ROCK in Rho-induced actin reorganization. *Nature cell biology* **1**, 136–143 (1999).
53. Brandizzi, F. et al. The destination for single-pass membrane proteins is influenced markedly by the length of the hydrophobic domain. *Plant Cell* **14**, 1077–1092 (2002).
54. Kessler, S. A., Lindner, H., Jones, D. S. & Grossniklaus, U. Functional analysis of related CrRLK1L receptor-like kinases in pollen tube reception. *EMBO Rep*. **16**, 107–115 (2015).
55. Thompson, M. V. & Wolniak, S. M. A plasma membrane-anchored fluorescent protein fusion illuminates sieve element plasma membranes in Arabidopsis and tobacco. *Plant Physiol* **146**, 1599–1610 (2008).
56. Vermeer, J. E. M., Van Munster, E. B., Vischer, N. O. & Gadella, T. W. J. Probing plasma membrane microdomains in cowpea protoplasts using lipidated GFP-fusion proteins and multimode FRET microscopy. *J. Microsc*. **214**, 190–200 (2004).
57. Ueda, T., Yamaguchi, M., Uchimiya, H. & Nakano, A. Ara6, a plant-unique novel type Rab GTPase, functions in the endocytic pathway of. *EMBO J*. **20**, 4730–4741 (2001).
58. Oda, Y., Nagashima, Y. & Fukuda, H. Reconstruction of ROP GTPase domains on the plasma membrane in tobacco leaves. *Methods Mol. Biol.* **1821**, 393–399 (2018).
59. Ryu, K. H., Huang, L., Kang, H. M. & Schiefelbein, J. Single-cell RNA sequencing resolves molecular relationships among individual plant cells. *Plant Physiol*. **179**, 1444–1456 (2019).
60. Zhang, Y. et al. The Class II KNOX family members KNAT3 and KNAT7 redundantly participate in Arabidopsis seed coat mucilage biosynthesis. *J. Exp. Bot.* **73**, 3477–3495 (2022).
61. Bhargava, A., Mansfield, S. D., Hall, H. C., Douglas, C. J. & Ellis, B. E. MYB75 functions in regulation of secondary cell wall formation in the Arabidopsis inflorescence stem. *Plant Physiol*. **154**, 1428–1438 (2010).
62. Ohashi-Ito, K., Oda, Y. & Fukuda, H. Arabidopsis VASCULAR-RELATED NAC-DOMAIN6 directly regulates the genes that govern programmed cell death and secondary wall formation during xylem differentiation. *Plant Cell* **22**, 3461–3473 (2010).
63. Cvrčková, F. Formins: emerging players in the dynamic plant cell cortex. *Scientifica (Cairo)* **2012**, 712605 (2012).
64. van Gisbergen, P. A. C. & Bezanilla, M. Plant formins: membrane anchors for actin polymerization. *Trends Cell Biol*. **23**, 227–233 (2013).
65. Ingouff, M. et al. Plant formin AtFH5 is an evolutionarily conserved actin nucleator involved in cytokinesis. *Nature cell biology* **7**, 374–U334 (2005).
66. Li, Y. et al. The type II Arabidopsis formin14 interacts with microtubules and microfilaments to regulate cell division. *Plant Cell* **22**, 2710–2726 (2010).
67. Liang, P. et al. Formin-mediated bridging of cell wall, plasma membrane, and cytoskeleton in symbiotic infections of Medicago truncatula. *Curr. Biol.* **31**, 2712–2719.e2715 (2021).
68. Diao, M. et al. formin 2 regulates cell-to-cell trafficking by capping and stabilizing actin filaments at plasmodesmata. *eLife* **7**, e36316 (2018).
69. Oulehlová, D. et al. Arabidopsis Class I Formin FH1 Relocates between Membrane Compartments during Root Cell Ontogeny and Associates with Plasmodesmata. *Plant Cell Physiol.* **60**, 1855–1870 (2019).
70. Ma, Z. M. et al. Formin nanoclustering-mediated actin assembly during plant flagellin and DSF signaling. *Cell reports* **34**, 108884 (2021).
71. Ma, Z. M. et al. Membrane nanodomains modulate formin condensation for actin remodeling in Arabidopsis innate immune responses. *Plant Cell* **34**, 374–394 (2022).
72. Takenaka, Y. et al. Patterned Deposition of Xylan and Lignin is Independent from that of the Secondary Wall Cellulose of Arabidopsis Xylem Vessels. *Plant Cell* **30**, 2663–2676 (2018).
73. Deeks, M. J. et al. The plant formin AtFH4 interacts with both actin and microtubules, and contains a newly identified microtubule-binding domain. *J. Cell Sci.* **123**, 1209–1215 (2010).
74. Kollárová, E., Forero, A. B., Stillerová, L., Prerostová, S. & Cvrcková, F. Arabidopsis Class II Formins AtFH13 and AtFH14 Can Form Heterodimers but Exhibit Distinct Patterns of Cellular Localization. *International journal molecular sciences* **21**, 348 (2020).
75. Gaillard, J. et al. Differential interactions of the formins INF2, mDia1, and mDia2 with microtubules. *Mol. Biol. Cell* **22**, 4575–4587 (2011).
76. Inoue, D. et al. Actin filaments regulate microtubule growth at the centrosome. *EMBO J.* **38**, e99630 (2019).
77. Martiniere, A., Gayral, P., Hawes, C. & Runions, J. Building bridges: formin1 of Arabidopsis forms a connection between the cell wall and the actin cytoskeleton. *Plant J.* **66**, 354–365 (2011).
78. Rosero, A. et al. Arabidopsis FH1 formin affects cotyledon pavement cell shape by modulating cytoskeleton dynamics. *Plant Cell Physiol.* **57**, 488–504 (2016).
79. Qin, Y. & Yang, Z. Rapid tip growth: insights from pollen tubes. *Semin. Cell Dev. Biol.* **22**, 816–824 (2011).
80. Guan, Y., Guo, J., Li, H. & Yang, Z. Signaling in pollen tube growth: crosstalk, feedback, and missing links. *Molecular plant* **6**, 1053–1064 (2013).
81. Cui, X., Zou, M. & Li, J. Basally distributed actin array drives embryonic hypocotyl elongation during the seed-to-seedling transition in Arabidopsis. *New Phytol.* **240**, 191–206 (2023).
82. Borassi, C. et al. An update on cell surface proteins containing extensin-motifs. *J. Exp. Bot.* **67**, 477–487 (2016).
83. Oda, Y. Cortical microtubule rearrangements and cell wall patterning. *Front. Plant Sci.* **6**, 236 (2015).
84. van Spoordonk, R., Schneider, R. & Sampathkumar, A. Mechanochemical regulation of complex cell shape formation: Epidermal pavement cells-A case study. *Quant Plant Biol.* **4**, e5 (2023).
85. Yan, Y., Sun, Z., Yan, P., Wang, T. & Zhang, Y. Mechanical regulation of cortical microtubules in plant cells. *New Phytol.* **239**, 1609–1621 (2023).
86. Huesmann, C. et al. Barley ROP binding kinase1 is involved in microtubule organization and in basal penetration resistance to the barley powdery mildew fungus. *Plant Physiol.* **159**, 311–320 (2012).
87. Nottensteiner, M., Zechmann, B., McCollum, C. & Huckelhoven, R. A barley powdery mildew fungus non-autonomous retrotransposon encodes a peptide that supports penetration success on barley. *J. Exp. Bot.* **69**, 3745–3758 (2018).
88. Nakamura, M. Microtubule nucleating and severing enzymes for modifying microtubule array organization and cell morphogenesis

in response to environmental cues. *New Phytol*. **205**, 1022–1027 (2015).
89. Klepikova, A. V., Kasianov, A. S., Gerasimov, E. S., Logacheva, M. D. & Penin, A. A. A high resolution map of the Arabidopsis thaliana developmental transcriptome based on RNA-seq profiling. *Plant J*. **88**, 1058–1070 (2016).
90. Adrian, J. et al. Transcriptome dynamics of the stomatal lineage: birth, amplification, and termination of a self-renewing population. *Developmental cell* **33**, 107–118 (2015).
91. Ramachandran, P. et al. Abscisic acid signaling activates distinct VND transcription factors to promote xylem differentiation in Arabidopsis. *Curr. Biol.* **31**, 3153–3161.e3155 (2021).
92. Hwang, B. G., Ryu, J. & Lee, S. J. Vulnerability of protoxylem and metaxylem vessels to embolisms and radial refilling in a vascular bundle of maize leaves. *Front Plant Sci*. **7**, 941 (2016).
93. Lassmann, T., Hayashizaki, Y. & Daub, C. O. TagDust-a program to eliminate artifacts from next generation sequencing data. *Bioinformatics* **25**, 2839–2840 (2009).
94. Langmead, B. & Salzberg, S. L. Fast gapped-read alignment with Bowtie 2. *Nat Methods* **9**, 357–359 (2012).
95. Li, H. et al. The sequence alignment/map format and SAMtools. *Bioinformatics* **25**, 2078–2079 (2009).
96. Cutler, S. R., Ehrhardt, D. W., Griffitts, J. S. & Somerville, C. R. Random GFP::cDNA fusions enable visualization of subcellular structures in cells of at a high frequency. *Proc. Natl. Acad. Sci. USA* **97**, 3718–3723 (2000).
97. Grefen, C. et al. A ubiquitin-10 promoter-based vector set for fluorescent protein tagging facilitates temporal stability and native protein distribution in transient and stable expression studies. *Plant J*. **64**, 355–365 (2010).
98. Nakagawa, T. et al. Improved gateway binary vectors: high-performance vectors for creation of fusion constructs in transgenic analysis of plants. *Biosci. Biotechnol. Biochem.* **71**, 2095–2100 (2007).
99. Sakamoto, S., Nomura, T., Kato, Y., Ogita, S. & Mitsuda, N. High-transcriptional activation ability of bamboo SECONDARY WALL NAC transcription factors is derived from C-terminal domain. *Plant Biotechnol (Tokyo)* **39**, 229–240 (2022).
100. Sakamoto, S. et al. Wood reinforcement of poplar by rice NAC transcription factor. *Sci. Rep.* **6**, 19925 (2016).
101. Pardee, J. D. & Spudich, J. A. Purification of muscle actin. *Methods Cell Biol*. **24**, 271–289 (1982).
102. Inoue, D., Ohashi, K., Takasuka, T. E. & Kakugo, A. In vitro synthesis and design of kinesin biomolecular motors by cell-free protein synthesis. *ACS Synth Biol*. **12**, 1624–1631 (2023).
103. Ursache, R., Andersen, T. G., Marhavy, P. & Geldner, N. A protocol for combining fluorescent proteins with histological stains for diverse cell wall components. *Plant J*. **93**, 399–412 (2018).
104. Dobin, A. et al. STAR: ultrafast universal RNA-seq aligner. *Bioinformatics* **29**, 15–21 (2013).
105. Robinson, M. D., McCarthy, D. J. & Smyth, G. K. edgeR: a Bioconductor package for differential expression analysis of digital gene expression data. *Bioinformatics* **26**, 139–140 (2010).
106. Tsutsui, H. & Higashiyama, T. pKAMA-ITACHI Vectors for Highly Efficient CRISPR/Cas9-Mediated Gene Knockout in. *Plant Cell Physiol*. **58**, 46–56 (2017).
107. Ursache, R., Fujita, S., Dénervaud Tendon, V. & Geldner, N. Combined fluorescent seed selection and multiplex CRISPR/Cas9 assembly for fast generation of multiple Arabidopsis mutants. *Plant Methods* **17**, 111 (2021).

Acknowledgements

We thank Dr. Nam-Hai Chua (Rockefeller University) for the pER8 vector, Dr. Tsuyoshi Nakagawa (Shimane University) for the pGWB vectors, Shigeo Sugano (AIST) for the pGTR vector, Dr. Anne Britt and Dr. Mily Ron (UC Davis) for the pDe vector, Dr. Satoshi Fujita (CNRS) for subcloned RCI2A, Dr. Kentaro Kobayashi (Hokkaido University) and Dr. Yuta Shimamoto (NIG) for TIRF microscopy, Dr. Taku Tsuyama (AIST) for technical support of imaging analysis, Dr. Yuki Ishikawa (Nagoya University) for technical support, Dr. Masayuki Takahashi for the actin purification, and the Bio Food Lab at Kyushu University for the use of facilities. This work was supported by MEXT KAKENHI (Grant nos. 19H05670, 19H05677 to Y.O., and 22H04720 to Y.K., 23H04425 to DI) and JSPS KAKENHI (Grant nos. 24K02042, 24H00056, 23K18126, 21H02514, JP22H04926 to YO, 20K22664, 24K18120 to SK, 23K23910 to YK, and 23K05801 to TS), NIG Postdoctoral Fellows (to SK), Japan Science and Technology Agency (JST) PRESTO (JPMJPR17Q1 to SI), and AMED Seeds-H (Grant nos. H26 to DI) and JST FOREST Program (grant no. JPMJFR224Q to YK). This work used the Vincent J. Coates Genomics Sequencing Laboratory at UC Berkeley, supported by NIH S10 OD018174 Instrumentation Grant.

Author contributions

Y.O. designed the research; S.K., T.S., Y.Ki. D.I., Y.Ko., M.Y. performed the experiments and data analysis; S.K., S.S., and N.M. contributed to the effector-reporter analysis; S.I. performed transcriptome analysis; S.K. and Y.O. wrote the manuscript.

Competing interests

The authors declare no competing interests.

Additional information

Supplementary information The online version contains supplementary material available at https://doi.org/10.1038/s41467-025-56866-y.

Correspondence and requests for materials should be addressed to Yoshihisa Oda.

Peer review information *Nature Communications* thanks Simon Turner and the other, anonymous, reviewer(s) for their contribution to the peer review of this work. A peer review file is available.